The volume of the 39.8 ka Campanian Ignimbrite, Italy

Aurora Silleni[1,1], Guido Giordano[2,2], Roberto Isaia[3,3], and Michael H Ort[4,4]

[1]University of Roma Tre
[2]Università degli Studi Roma Tre
[3]Istituto Nazionale di Geofisica e Vulcanologia, sezione di Napoli Osservatorio Vesuviano
[4]Northern Arizona University

November 30, 2022

Abstract

The 39.8 ka Campanian Ignimbrite (CI) is the largest caldera-forming eruption of the Campi Flegrei during the Quaternary, which had a global-scale impact on the environment and human populations. The cooling following the eruption and the several effects of it strongly affected the paleoenvironment and the migration of hominids in Europe. The volume of the eruption is necessary to constrain the climate model of this area in the past. However, despite a large number of studies, the Dense Rock Equivalent (DRE) volume estimates range from 60 to 300 km. Here we present a review of the previous volume evaluations and a new calculation of the volume of the ignimbrite. This estimate is constrained by an isopach map that reconstructs the paleo-topography during the eruption. The preserved total bulk extra-caldera volume of the ignimbrite is estimated at 61.5 km ± 5.5 km. The total PDC deposit volume is then corrected for erosion, ash elutriation, the intracaldera deposit volume and the volume of tephra deposited in the sea. The total final volume estimate of the eruption ranges from 164.9 km – 247.7 km DRE. This value corresponds to a mass of 4.30 - 6.46 x 10 kg, a magnitude (M) of 7.7 and a VEI of 7. This M makes the CI the largest-magnitude Quaternary eruption in the Mediterranean area. The new detailed estimation of CI eruption physical parameters confirms this event as capable of having significantly affected human activity and the environment on a large scale at the time of the eruption.

The volume of the 39.8 ka Campanian Ignimbrite, Italy

Aurora Silleni[1#], Guido Giordano[1], Roberto Isaia[2], Michael H. Ort[3]

 # corresponding author: aurora.silleni@uniroma3.it

1- Dipartimento di Scienze, Università di Roma Tre, Largo S. Leonardo Murialdo 1, 00146, Rome, Italy

2- Istituto Nazionale di Geofisica e Vulcanologia, Osservatorio Vesuviano, Via Diocleziano 328, 80124 Naples, Italy

3- SES, Box 4099, Northern Arizona University, Flagstaff, AZ 86011-4099, USA

Key Points

- The preserved extra-caldera bulk volume of the ignimbrite is 61.5 km^3 ± 5.5 km^3.
- The eruption had a total volume of 164.9 km^3 – 247.7 km^3 DRE and a magnitude of 7.7.
- The volume is essential for climate simulations of Europe during the Pleistocene.

Abstract

The 39.8 ka Campanian Ignimbrite (CI) is the largest caldera-forming eruption of the Campi Flegrei during the Quaternary, which had a global-scale impact on the environment and human populations. The cooling following the eruption and the several effects of it strongly affected the paleoenvironment and the migration of hominids in Europe. The volume of the eruption is necessary to constrain the climate model of this area in the past. However, despite a large number of studies, the Dense Rock Equivalent (DRE) volume estimates range from 60 to 300 km^3. Here we present a review of the previous volume evaluations and a new calculation of the volume of the ignimbrite. This estimate is constrained by an isopach map that reconstructs the paleo-topography during the eruption. The preserved total bulk extra-caldera volume of the ignimbrite is estimated at 61.5 km^3 ± 5.5 km^3. The total PDC deposit volume is then corrected for erosion, ash elutriation, the

intracaldera deposit volume and the volume of tephra deposited in the sea. The total final volume estimate of the eruption ranges from 164.9 km^3 – 247.7 km^3 DRE. This value corresponds to a mass of 4.30 - 6.46 x 10^{14} kg, a magnitude (M) of 7.7 and a VEI of 7. This M makes the CI the largest-magnitude Quaternary eruption in the Mediterranean area. The new detailed estimation of CI eruption physical parameters confirms this event as capable of having significantly affected human activity and the environment on a large scale at the time of the eruption.

Plain Language Summary

The Campanian Ignimbrite is the most powerful eruption of Campi Flegrei, Italy, occurred around 40,000 of years ago. It developed a huge pyroclastic density current, a flow of ash, rocks and gas at elevated temperature and velocity, the most dangerous process related to volcanic eruptions. The rocks generated by the flow (the ignimbrite) are located far from the caldera (up to 80 km), indicating the high energy of the eruption. In this work, the thickness of this ignimbrite is reported on an isopach map, which helps to calculate the volume of the ignimbrite and to understand the processes related to the flow. We estimate the volume of the magma of the eruption (from 164.9 km^3 to 247.7 km^3) and the total mass of magma (4.30 - 6.46 x 10^{14} kg), correspond of around 80 million of Olympic-size swimming pools and the weight of 102 billion of elephants. We classify this eruption as a Volcanic Explosive Index of 7 on a maximum of 8, which defines it as the largest eruption occurred in the Mediterranean area in the past. The volume is also important to model the climate impact of this natural disaster that affected the human population of that time.

Index Terms

8428 Explosive volcanism (4302); 8408 Volcano/climate interactions (1605, 3309, 4321); 8414 Eruption mechanisms and flow emplacement; 8486 Field relationships (1090, 3690); 8404 Volcanoclastic deposits.

Keywords

Campanian Ignimbrite; Campi Flegrei; Isopach maps; Ignimbrite volumes; Pyroclastic density currents; Super-eruption.

1. Introduction

Pyroclastic density currents (PDCs) have large impacts on human communities and the environment; they can cause catastrophic environmental and property damage and loss of life, as well as accounting for the major proportion of deaths caused by volcanic activity. In the last 200 years, 26.8% of volcano-induced mortality resulted from PDCs (Tanguy et al., 1998; Witham, 2005). Moreover, global and regional climatic effects can result from the injection of ash and sulfur aerosols into the stratosphere during large explosive eruptions, leading to a "volcanic winter" (Rampino and Self, 1992; Stuiver et al., 1995; Thordarson and Self, 1996). The quantitative computation of the size of explosive eruptions is essential to understand their potential impact on humans, climate and ecosystems (Mason et al., 2004). Calculating the volume of volcanic large eruptions is necessary to define the size and to model the climate effects of these natural phenomena occurred in the past.

The total eruptive product of large caldera-forming eruptions can consist of both fall deposits and ignimbrites (Parfitt & Wilson, 2008), and typically the largest proportion is transported in PDCs and emplaced as ignimbrites. Numerical models have greatly improved estimates of tephra dispersal from the fallout phase in recent years (Barsotti et al., 2008; Bonadonna et al., 1998, 2005; Bonadonna & Phillips, 2003; Costa et al., 2006, 2012; Folch, 2012; Folch et al., 2010). However, at present, a clear "reference" method for the calculation of ignimbrite volume does not exist and uncertainties on such computations are huge (Mason et al., 2004). The volume of ignimbrites is difficult to evaluate due to the irregularity of the ignimbrite surface, the variable thickness (controlled by the paleomorphology), the effect of erosion, the presence of younger products and the variable density of the deposits.

The Campanian Ignimbrite (CI; Barberi et al., 1978; De Vivo et al., 2001; Fedele et al., 2008; Fisher et al., 1993) is associated with the most powerful caldera-forming eruption from Campi Flegrei (Fig. 1a) (Rosi & Sbrana, 1987; Perrotta et al., 2006; Scarpati et al., 2013), which occurred at 39.8 ka (Giaccio et al., 2017). It is one of the largest late Quaternary explosive events and has been considered as an example of a super-eruption (Sparks et al., 2005). The CI tephra represents the most widespread volcanic deposit and one of the most important temporal/stratigraphic markers for the Early Upper Paleolithic of western Eurasia (F. G. Fedele et al., 2003; Giaccio et al., 2008; Pyle et al., 2006). The eruption may have affected human residents in different

ways: by destroying the animal and human populations, by altering the species composition and growth rhythm and by changing the availability of water (F. G. Fedele et al., 2002, 2007; Lowe et al., 2012). The abrupt volcanic cooling following the eruption occurred in a more intense way in Eastern Europe and Northern Asia, and reached from -6°C up to -9°C. The cooling could have influenced the migration of the populations and have affected the daily life for Neanderthals and modern humans during the Middle to Upper Paleolithic transition (Black et al., 2015; Marti et al., 2016).

In this work, we present a review of all papers that determined the CI volume. Despite the large number of studies, the estimates of total Dense Rock Equivalent (DRE) volume of CI range from 60 to 300 km^3, with no apparent convergence on an accepted value (Civetta et al., 1997; Cornell et al., 1983; Costa et al., 2012; F. G. Fedele et al., 2003; Fisher et al., 1993; Giaccio, 2006; Marianelli et al., 2006; Marti et al., 2016; Pappalardo et al., 2008; Perrotta & Scarpati, 2003; Pyle et al., 2006; Rolandi et al., 2003; Rosi et al., 1983, 1999; Scarpati et al., 2014; Thunell et al., 1979). The volume of distal tephra (both Plinian and co-ignimbrite) is well defined due to the many measurements across the vast region and a recent improvement of computational methods (Costa et al., 2012; Marti et al., 2016). Nevertheless, the volume of the PDC deposits was never calculated by direct measurements. We propose a rigorous method to develop the isopach map of the Campanian Ignimbrite based on mapping of the preserved deposits and the reconstruction of the paleomorphology, especially in mountain areas. We provide a revised volume of the pyroclastic density current extra-caldera deposits of the CI preserved on land based on a verifiable method of calculation. Using this as a base, we correct for erosion, elutriation, intracaldera volume and underwater deposits to calculate the most reliable total bulk and Dense Rock Equivalent (DRE) volumes for this eruption. The obtained volume strongly reduces the total error in the previous estimates, which should be used to better develop and constrain the climate model of the Eastern Europe during the Paleolithic period.

2. Volcanological background

The activity in the Campi Flegrei began prior to 80 ka (Pappalardo et al., 1999; Scarpati et al., 2013). The area consists of two nested depressions formed and activated during both the CI and the more recent ~15 ka Neapolitan Yellow Tuff (NYT) eruptions (Acocella, 2008; Orsi et al., 1996; Perrotta et al., 2006; Vitale &

105 Isaia, 2014; Di Vito et al., 1999). A recent study identified an M 6.6 event correlated to the Y-3 tephra, named
106 Masseria del Monte Tuff; this eruption is likely to have generated a caldera collapse between CI and NYT
107 (Albert et al., 2019). After the NYT eruption, intra-caldera volcanic activity continued with more than 70
108 eruptions, subdivided into three volcanic epochs: epoch I (15-10.6 ka), epoch II (9.8-9.2 ka) and epoch III (4.6-
109 3.8 ka) (Isaia et al., 2009; Smith et al., 2011; Di Vito et al., 1999). The last eruption occurred in 1538 CE and
110 led to the formation of the Monte Nuovo tuff cone.

111 The CI eruption emplaced both pyroclastic fall and PDC deposits in a complex sequence currently exposed in
112 proximal, medial, distal and ultra-distal outcrops (Fig. 1) (Barberi et al., 1978; Cappelletti et al., 2003; Engwell
113 et al., 2014; L. Fedele et al., 2008; Fisher et al., 1993; Orsi et al., 1996; Perrotta et al., 2006; Perrotta & Scarpati,
114 1994, 2003; Rosi et al., 1988, 1996, 1999; Scarpati et al., 2015a, 2015b; Scarpati & Perrotta, 2016; Smith et
115 al., 2016; Sparice, 2015; De Vivo et al., 2001). The first phase of the eruption generated a Plinian column up
116 to 44 km high (Marti et al., 2016; Rosi et al., 1999), producing a widespread fall deposit dispersed by winds
117 to the east (Marti et al., 2016; Perrotta & Scarpati, 2003; Rosi et al., 1999; Scarpati & Perrotta, 2016). A
118 pyroclastic density current then spread over an area of 7,000 km^2 and surmounted ridges more than 1,000 m
119 high (Barberi et al., 1978; Fisher et al., 1993). This stage caused the caldera collapse and the accumulation of
120 lithic breccia's deposits (Breccia Museo) in scattered outcrops along the caldera rim (L. Fedele et al., 2008;
121 Melluso et al., 1995; Perrotta & Scarpati, 1994; Rosi et al., 1996). In distal outcrops, most of the CI is
122 represented by a massive, gray ignimbrite (Barberi et al., 1978; Fisher et al., 1993; Scarpati et al., 2015a;
123 Scarpati & Perrotta, 2012). In more distal and ultra-distal sites deposits are made up by coarse to fine ash
124 containing both co-plinian and co-ignimbrite tephra (Engwell et al., 2014; Smith et al., 2016; Sparks & Huang,
125 1980; Thunell et al., 1979). The tephra marker related to this eruption is essential to correlate volcanological
126 and archeological sites in the Mediterranean area and Eastern Europe. Tephra-based correlations of human
127 sites were used to date the Middle to Upper Paleolithic transition (Lowe et al., 2012).

128 The complex stratigraphy of this eruption differs between proximal and distal outcrops (Fig. 1b, Fig. 1c).
129 Moreover, it is difficult to study the lateral correlations due to the absence of outcrops in medial areas (except
130 for the Lago di Patria outcrop, Table A2 in Data Repository), because all quarry-pits have been refilled. The
131 limited drill core data shows little evidence of lateral unit change. In our study, we refer to the stratigraphic
132 units proposed by Fedele et al. (2008) (proximal area) and Cappelletti et al. (2003) (medial and distal areas).

The stratigraphy in proximal areas, from bottom to top, consists of 6 units: 1) Plinian pumice fallout deposit (PPF); 2) unconsolidated stratified ash flow (USAF); 3) welded gray ignimbrite (WGI) interlayered with some more welded levels (Piperno); 4) lower pumice flow unit (LPFU); lithic breccia unit (BU), in places with welded spatter beds (SU); and 6) upper pumice flow unit (UPFU). The stratigraphic sequence of distal outcrops involves, from bottom to top: 1) PPF; 2) USAF; 3) WGI; 4) lithified yellow tuff (LYT); and 5) coarse pumice flow (CPF).

3. The previous estimates of the CI volume

Define the eruptive volume is necessary to simulate the climate impact of this eruption in Eastern Europe. Here is reported a review of the previous estimates of the CI volume aim to define a constrained volume for this eruption.

The total volume erupted during a caldera-forming eruption, like the CI, is composed of the mass ejected during the phases that produced Plinian columns (V_{pf}), and pyroclastic density currents (V_{pdc}) (1):

$$V = V_{pf} + V_{pdc} \quad \text{[eq. 1]}$$

Both V_{pf} and V_{pdc} are made of the main primary deposits (respectively the Plinian fallout V_{ppf} and the ignimbrite V_i) and their associated co-plinian fall (V_{cpf}) and co-ignimbrite ash fall (V_{ci}). Consequently (2):

$$V = V_{ppf} + V_{cpf} + V_i + V_{ci} \quad \text{[Eq. 2]}$$

All these four factors were calculated during the last forty years by different authors and with different methods (Table 1), resulting in final dense rock equivalent (DRE) volume estimates ranging from 60 to 300 km^3 (Civetta et al., 1997; Cornell et al., 1983; Costa et al., 2012; F. G. Fedele et al., 2003; Fisher et al., 1993; Giaccio, 2006; Marianelli et al., 2006; Marti et al., 2016; Pappalardo et al., 2008; Perrotta & Scarpati, 2003; Pyle et al., 2006; Rolandi et al., 2003; Rosi et al., 1983, 1999; Scarpati et al., 2014; Thunell et al., 1979).

Due to the difficulty to distinguish the contribution of the co-plinian fall and the co-ignimbrite ash fall in ultra-distal locations, some authors simply refer to the widespread Y-5 ash layer, which comprises both. This layer is the tephra marker linked to the CI eruption and is recognized from marine cores across the Eastern Mediterranean region to Russia, for this reason, Y-5 is an excellent chronostratigraphic marker in the Northern Hemisphere (Cornell et al., 1983; Engwell et al., 2014; F. G. Fedele et al., 2003; Giaccio et al., 2006; Narcisi

& Vezzoli, 1999; Pyle et al., 2006; Smith et al., 2016; Thunell et al., 1979; Ton-That et al., 2001). Previous studies distinguished also the co-plinian and co-ignimbrite contribution (Marti et al., 2016; Perrotta & Scarpati, 2003; Smith et al., 2016; Sparks & Huang, 1980); some of them calculated the relative volume and the associated method of calculation will be discussed later (Marti et al., 2016; Perrotta & Scarpati, 2003).

The first volume estimate of the ignimbrite was presented by Thunell et al. (1979). Based on a geometrical method that considers a covered area of over 6000 km^2 with a thickness up to 100 m and assuming a radial flow of the PDC, they estimate the DRE volume is at least 30-40 km^3. The DRE volume of the Y-5 ash layer within the 1-cm isopach contour was also estimated at 30-40 km^3 (65 km^3 bulk) and the authors recognized that Y-5 is composed by a co-plinian and a co-ignimbrite ash, but they did not calculate each contribution to the volume. Their total DRE volume is 60-80 km^3 for the eruption.

Cornell et al. (1983) calculated the ash-fall layer volume of Y-5 from an isopach map derived by different cores drilled in the Mediterranean Sea (73 km^3 bulk). They then included the ignimbrite DRE volume proposed by Thunell et al. (1979) in their overall eruption volume estimate.

Fisher et al. (1993) estimated a bulk volume of the original pyroclastic current of about 500 km^3 by circumscribing a circle of deposits with a radius of 100 km, 100 m thick at the center that thinned to zero at the perimeter of the circle.

Civetta et al. (1997) is one of the first works that subdivided the volume of the CI based on the pumice composition. The authors divided the magma into three different types: a most evolved one that consists of Plinian fallout and some ignimbrite up to 50 km from the vent (a volume of 25 km^3 DRE), a magma with intermediate composition that includes some of the ignimbrite out to its farthest extent (100 km^3 DRE), and a least-evolved magma that includes much of the ignimbrite in the Campanian Plain (20 km^3 DRE). All the volume calculations were made by circumscribing circles with a radius similar to the maximum distance reached from the vent by that magma type and a thickness that goes from the maximum thickness of ignimbrite of that composition at the caldera center to zero at the perimeter of the circle.

Pappalardo et al. (2008) used petrological data to constrain the pre-eruptive magma storage dynamics and, in agreement with Civetta et al. (1997), proposed a total volume of 200 km^3 DRE (20 km^3 for the fallout and 180 km^3 for the ignimbrite).

Rosi et al. (1999) calculated the bulk volume of the Plinian fallout as 15 km^3 based on the method proposed by Pyle (1989), which assumes exponential thickness decay away from the vent and an elliptical isopach distribution with the source at one focus; in the CI case, this focus corresponds to a central vent, located in the Campi Flegrei caldera center (town of Pozzuoli). The same technique was used by Perrotta and Scarpati (2003), who estimated a bulk volume of 4.03 km^3, the different value being the result of a different way than Rosi et al. (1999) used to trace the isopach lines. In the same work, the authors attempt, for the first time, to discriminate between the co-plinian and co-ignimbrite components. The coarse ash of ultra-distal deposits was interpreted as the co-plinian phase, while the fine ash represents the co-ignimbrite component. The authors evaluated the thicknesses of the two parts and estimated the volume as follows: 16 km^3 of co-plinian ash and 100 km^3 of co-ignimbrite ash. Scarpati and Perrotta (2016) subdivided the fallout into five layers (A to E) and calculated the volumes for each of them using the same exponential fitting, obtaining a primary fallout of 5.33 km^3 (0.88 km^3 DRE) and a co-plinian ash of 14.67 km^3 (6.88 km^3 DRE).

These analyses were improved upon by Pyle et al. (2006), who estimated the minimum bulk volume of the CI fallout of 74 km^3 or 31 km^3 DRE: the authors used the general observation that many fallout deposits show exponential decay of thickness (Pyle, 1989) and formulated that the total volume of the exponentially thinning sheet is equal to $13.08T_0b_t^2$ (T_0 is the maximum thickness at source and b_t is the linear distance over which the isopach thickness falls by a half). In the same work, the authors compared these results with a second approach based on the rate of thinning of the distal ash sheets (Pyle, 1989, 1990): given that the thickest ash layer in marine cores is of the order of 10–20 cm, it is most likely that the total bulk ash volume associated with the eruption was in the range 74-120 km^3 (31–50 km^3 DRE) (Pyle et al., 2006).

A first attempt to compare all the volume estimates was proposed by Fedele et al. (2003), who considered the sum of the conservative estimates reported in literature. The total DRE volume they proposed is 200 km^3 (the sum of the fallout, the PDC deposits and the Y-5 ash layer volumes (Civetta et al., 1997; Rosi et al., 1999; Thunell et al., 1979)).

Giaccio (2006) calculated the volume of the PDC using a complex truncated cone, with a concave surface and variable heights: 70 m up to 10 km from the center, 50 m up to 20 km, 20 m up to 45 km and 0 m up to 100 km. The volume obtained is 385 km^3 (215 km^3 DRE). At the same time, he proposed a revised isopach map

for the fallout deposits, resulting in a volume estimate of 10 km^3 (3 km^3 DRE). Moreover, combining all available data on the distal tephra of CI from the literature (Castagnoli et al., 1995; Cornell et al., 1983; McCoy & Cornell, 1990; Melekestsev et al., 1984; Narcisi & Vezzoli, 1999; Paterne et al., 1986; Seymour & Christanis, 1995; Seymour et al., 2004; Ton-That et al., 2001; Upton et al., 2002), Giaccio (2006) calculated the volume of this fraction as 180 km^3 (86 km^3 DRE). He thus estimated a bulk volume of 575 km^3 (300 km^3 DRE).

The most difficult part of drawing isopach maps of the Plinian fallout is the limited number of distal subaerial locations where the tephra is found. To solve this, a new volume estimate was proposed by Costa et al. (2012) based on the fit of an advection – diffusion tephra dispersion model to thickness data. They obtained a bulk volume of the tephra of 250-300 km^3 (104-125 km^3 DRE) and a total volume of the eruption of 430-680 km^3 (180-280 km^3 DRE).

An innovative method for estimating the PDC volume was used by Scarpati et al. (2014). They applied equation (3) to calculate the ignimbrite volume assuming a co-ignimbrite volume (V_{ci}) of 100 km^3 obtained by Perrotta and Scarpati (2003) and a mean vitric loss of 0.65. The method is based on the enrichment factor of Walker (1972, 1980) and the vitric loss of the ignimbrite proposed by Sparks and Walker (1977). The volume (V) (3) is equal to:

$$V = V_{ci}/vitric\ loss - V_{ci} \qquad \text{[Eq. 3]}$$

The bulk volume of the PDC deposits thus estimated is 54 km^3 (25 km^3 DRE). In the same study, the authors proposed a review of the previous volume estimations (Scarpati et al., 2014).

The most recent work on the fallout volume was presented by Marti et al. (2016). The authors recognized two distinct plume phases: the Plinian and the co-ignimbrite fall. They applied a computational inversion method that explicitly accounts for the two phases and for gravitational spreading of the umbrella cloud. The Plinian fallout bulk volume thus calculated is 54 km^3 (22.6 km^3 DRE) and the co-ignimbrite bulk volume is 153.9 km^3 (61.6 km^3 DRE), for a bulk total volume of 207.9 km^3 (84.2 km^3 DRE).

To summarize, the existing estimates of the total DRE volume of the CI eruption range from 60 to 300 km^3 (Civetta et al., 1997; Cornell et al., 1983; Costa et al., 2012; F. G. Fedele et al., 2003; Fisher et al., 1993;

239 Giaccio, 2006; Marianelli et al., 2006; Marti et al., 2016; Pappalardo et al., 2008; Perrotta & Scarpati, 2003;
240 Pyle et al., 2006; Rolandi et al., 2003; Rosi et al., 1983, 1999; Scarpati et al., 2014; Thunell et al., 1979) and
241 those for the bulk volume of the CI pyroclastic density current deposits range between 54 and 500 km^3 (Civetta
242 et al., 1997; Cornell et al., 1983; Fisher et al., 1993; Marianelli et al., 2006; Pappalardo et al., 2008; Rolandi
243 et al., 2003; Scarpati et al., 2014; Thunell et al., 1979). The margin of error in these volumes is unacceptably
244 high due to the different methods used, especially in view of the relevance of such figures on the impact on
245 climate and the environment. While the computational methods for the fallout deposits have improved
246 significantly in the past ten years and the related figures for the fallout phase appear strong and solidly based
247 on field data (Costa et al., 2012; Marti et al., 2016), the volume figures for the CI ignimbrite appear to remain
248 very poorly constrained, although this volume largely affects the estimation of the volume of elutriated co-
249 ignimbrite ash, which is the dominant fallout phase across Europe and the most relevant fraction of ash injected
250 into the stratosphere at the time of the eruption (e.g. Costa et al., 2018).

251

252 **4. The making of the CI isopach map**

253 In order to reduce this wide range in volume estimates, we focus on constraining the volume of the PDC
254 deposits of the CI. Our calculation of thickness and volume does not take into account the initial pyroclastic
255 Plinian fall phase and the co-ignimbrite fallout; we used the fall volume calculation of other authors, the
256 maximum and the minimum proposed in literature by Perrotta and Scarpati (2003) and Marti et al. (2016). Our
257 CI isopach map is based on previous published data, fieldwork and the assessment of the paleo-topographic
258 control exerted on the deposits thickness distribution.

259

260 *4.1 Database and fieldwork*

261 Published data regarding CI thickness and outcrop locations were collected from 42 papers (presented in Data
262 Repository, Table 1). The whole data were inserted in a GIS Open-Source QGIS 3.4
263 (https://www.qgis.org/it/site/) database including 238 localized outcrops. The database includes the name of
264 the location, the lithological description, the geographic coordinates, the elevation a.s.l., the thickness of the
265 flow units (specifying whether total or outcrop thickness), the maximum lithic dimensions and the degree of

266 welding. Where both base and top of the CI are exposed, the thickness is classified as total and elsewhere it is
267 considered a minimum thickness.

268 This database has been augmented by our field data acquired in 97 locations (presented in Data Repository,
269 Table 2), both in proximal and distal areas (Fig. 1d). Fieldwork was aimed to measure the total or minimum
270 thickness, the local stratigraphy and to understand the relation of the ignimbrite with the topography.

271

272 *4.2 The zero-thickness isopach*

273 The zero-thickness isopach is an outer limit beyond which the CI is not present, and it delimits the current
274 areal distribution of the PDC outcrops. The isopach was reconstructed through a first phase of revision of the
275 geological maps already existing at the scale 1:10,000, 1:50,000 or 1:100,000 (ISPRA, 2009, 2010, 2011a,
276 2011b, 2011c, 2011d, 2014a, 2014b, 2016, 2018; Rosi & Sbrana, 1987; Sbrana & Toccaceli, 2011; Servizio
277 Geologico d'Italia, 1963, 1965a, 1965b, 1965c, 1966, 1967a, 1967b, 1971a, 1971b, 1975; Vezzoli & Barberi,
278 1988). The contact was traced between the CI and older units and extrapolated where CI does not crop out. In
279 this circumstance, the ignimbrite is generally covered by younger deposits, but it is necessary to assess if the
280 CI was never emplaced there. To distinguish between these two cases, a statistical and morphological analysis
281 of the actual slope of the top of the CI was applied and a comparison between the topography and the average
282 slope of the CI top was carried out. Where the slope angle is comparable, the area was included in the zero-
283 thickness isopach, even if CI is not cropping out. Greater slope angles were attributed to underlying basement
284 (mostly Meso-Cenozoic calcareous or flysch) and the isopach was traced to leave out these areas and no
285 primary CI deposition was interpreted.

286

287 *4.3 The isopachs*

288 To determine the isopach locations, two different methods were used, one in the proximal area (from the
289 caldera to the base of the Apennine Mountains, including the Campanian Plain) and one in the more distal
290 area. The almost complete lack of outcrops in the Campanian Plain and the valley-ponded depositional style
291 in the ridge-valley topography of the Apennine Mountains (L. Fedele et al., 2016; Langella et al., 2013; Perrotta

et al., 2010; Rosi et al., 1983, 1996; Scarpati et al., 2014, 2015a; Sparice, 2015) make these different approaches necessary.

In the proximal area, data from the literature (Bellucci, 1994; ISPRA, 2011d; Milia and Torrente, 2007; Ortolani and Aprile, 1985; Rolandi et al., 2003; Scandone et al., 1991; Torrente et al., 2010), consisting of more than 300 thickness values of CI from boreholes, outcrops and geological sections were used to fit isopachs on the map. In the distal area, the isopach locations were based upon our field observations and the reconstruction of the pre-CI topography (Fig. 2). A series of profiles in the Apennine Mountains were drawn to outline the trend of the valleys (Fig. 2b). The coast-line in Mediterranean Sea at the time of the CI emplacement (39.8 ka) was lower than present-day, but it is difficult to define the precise level due to the high tectonic activity in the region and the difference in behavior between a closed basin such as the Mediterranean Sea and the Atlantic Ocean, which responded predictably to global sea-level changes. Based upon limited sea-level correlation work in the Mediterranean basin (Antonioli, 2012; Antonioli et al., 2004; Lambeck & Bard, 2000), we assumed a sea level between 75 m and 87 m lower than present-day.

Topographic cross-sections were traced orthogonally to the center of the valley and to the contour lines, including the flanks of the reliefs and the zero-thickness isopach. The slopes of the valley above the CI zero isopach were extended and gradually shallowed toward the valley center in order to reconstruct the paleo-valley with an inclination of the sides similar to the current slope, always taking into consideration the geological and morphological features (Fig. 2c), and assuming that the Meso-Cenozoic mountain slopes have not significantly changed since 40 ka. The CI typically has a valley-pond geometry inside the Apennine Mountains (L. Fedele et al., 2016; Perrotta et al., 2010; Rosi et al., 1996; Scarpati et al., 2014, 2015a; Sparice, 2015). The base elevation of the paleo-valleys is constrained by field data where the CI base has been measured.

These reconstructed valleys culminate generally in a V shape, with the bottom elevation, above the sea level, for each profile representing the paleo-valley floor. All these elevations represent the ancient pattern of the valley bottom, for this reason, they were modified if they were inconsistent with the progressive downslope decrease in elevation. We also took into account the slope of the present-day drainage network (Fig. 2a).

Finally, the neo-incision of rivers in the profiles was flattened, to not include in the result the linear erosion of the last 39.8 ka (Fig. 2c). The CI thickness is calculated by these modified profiles, and it is always constrained by field data on the CI thickness and with the geological maps. These thickness values are then reported on the isopach map.

All the isopachs were traced always in coherence with field data, for both thickness and base elevation, geology of Meso-Cenozoic sides of the valleys and, finally, the progressive downslope decrease in the base elevation of the valleys referred to the present-day drainage network. Where these data were not consistent, an adjustment in some profiles was necessary. The most significant adjustments were made for a resulting over-thickening inside the valleys. In these cases, the thickness was modified in coherence with fieldwork.

5. Results

We use, as starting point for the volume estimation, the PDC volume, obtained from the detailed isopach map. From the previous review, it is evident that this information lacks in previous works on the CI volume. Here, we refer to all PDC units of the CI, that in the medial and distal outcrops are mainly composed by WGI. Density and porosity data are used to define the DRE volume.

5.1 The isopach maps

The statistical and morphological analysis of the upper surface of the CI used 48804 points throughout the areal extension of the deposits (both in proximal and distal areas). This analysis shows that 64% (31057) of the points have slopes lower than 5°. Moreover, 80% of the points have slopes lower than 10° and 99% have a surface slope lower than 55° (Fig. 3). This is in agreement with the observation on the slope of the top surface of the valley-ponded Taupo Ignimbrite, which is around 8° (Wilson & Walker, 1985).

Based on these results, the 0-m isopach was traced to enclose all the mapped CI and areas that probably have the CI below the recent sedimentary cover and have a slope less than 15°. The total area enclosed by the 0-m isopach of the CI is 3216 km^2 (Fig. 4). To understand also the total area of the region involved in the PDC, a

shape was drawn comprising all the areal extension of the isopach 0-m. The enveloped area is equal to 7547 km^2, similar to the 7000 km^2 estimate (Barberi et al., 1978).

The isopach map traced in the proximal area does not include the intracaldera deposits. The maximum thickness in proximal areas is 80 m (Fig. 5), mainly based on outcrops near the caldera rim; the CI thins gradually away from the caldera margin. Two areas of thickening are identified just north of the caldera and east of Lago Patria (up to 70 m) and in the area of Casoria (up to 50 m) (Fig. 6a). Three main areas of thinning (down to 10 m) are recognized to the north in the Campanian Plain (Fig. 6b), in the area between Aversa and Acerra and in the south of the Campanian Plain (Fig. 6a).

Two thickened portions are on the northern side of the Campanian Plain (north-east of Mondragone) (Fig. 6b) and on the eastern side (from Caserta to Maddaloni) (Fig. 6c), both just in front of the first Apennine ridges.

The isopach for the distal reaches has a maximum thickness of 50 m in the area of Maddaloni Valley (Fig. 6c). A series of confined valleys show local thickening. These include, from northwest to southeast, Mortola (up to 30 m), Roccamonfina (up to 30 m) (Fig. 6d), San Lorenzello and all the Volturno plain (up to 20 m) (Fig. 6e), Sant'Agata dei Goti (up to 40 m), Tufara (up to 20 m), Monteforte Irpino and Avellino (up to 30 m) (Fig. 6f), Tramonti (up to 10 m) and Sorrento (up to 20 m) (Fig. 6g).

5.2 Density of the CI deposits

More than 40 samples from different outcrops scattered around the Campanian Plain were analyzed to determine their density. Samples were cut in cylinders (with radius between 0.9 cm and 2 cm and height between 0.8 and 5.7 cm) or cubes (sides from 0.8 to 2.5 cm) and analyzed using a Micromeritics AccuPyc II 1340 helium pycnometer. The resulting density was used to interpret total and open porosity, the density is used to determine the DRE volume.

The bulk density (ρ) of the WGI samples from the Campanian Plain ranges from 0.745 ± 0.015 g/cm^3 to 1.330 ± 0.003 g/cm^3, with an average at 0.980 ± 0.011 g/cm^3. The bulk density of the Piperno unit ranges from 1.275 ± 0.008 g/cm^3 to 1.302 ± 0.002 g/cm^3, with an average of 1.287 ± 0.004 g/cm^3 (presented in Data Repository, Table 3). Open porosity was estimated with geometric (V_g) and matrix volume (V_m): $100*(V_g-V_m)/V_g$, while closed porosity was determined using the DRE of the WGI and Piperno powder, which was obtained by the

pycnometer. The total WGI porosity (φ_t) was calculated directly adding up closed and open porosity and it ranges from 49 ± 5% and 71± 5% and the average is 61.6% ± 5%, for the Piperno unit it is 50 ± 1%. The ρ DRE is 2.6077 ± 0.0031 g/cm^3. The DRE volume is determined multiplying the bulk volume by (100- φ_t)/100.

5.3 Deposits volume calculation

The area enclosed by each isopach, reported in Fig. 7, allows the CI volume to be calculated. This is the subtended area of the plot thickness-cumulative area (Walker, 1980, 1981); the area of each isopach was calculated directly from the QGIS software. Table 2 displays the values of the area and the volume for each isopach. The largest part of the volume is relative to deposits thicknesses <10 m (60.52%), whereas the isopachs from 40 m to 80 m contain less of the 10% of the total volume (7.17%).

The total volume of the preserved extra-caldera CI deposits on land is 61.5 km^3 ± 5.5 km^3 (22.0 ± 2.2 km^3 DRE).

To understand the extra-caldera volume subdivision in proximal and distal areas, the isopach map is portioned in two parts, one comprising all the Campanian Plain, and the other from the first Apennine ridges to the final runout (Fig. 5). The resulting extra-caldera volumes are 46.4 ± 1.6 km^3 in the proximal area (~75%) and 15.1 ± 3.9 km^3 in the distal area (~25%); the sources of error and the uncertainties are due to the methods used and their calculation is explained in Supporting Information.

A recent study proposed contour maps of the lower and the upper surfaces of the CI for the north-western sector of the proximal area, based on 1000 of lithostratigraphic logs from boreholes (Ruberti et al., 2020). The difference of the upper surface and the lower one is the CI thickness, which is not reported on the work of Ruberti et al. (2020). The extrapolated thicknesses from the maps were compared with the isopach map of the proximal area of this work and it shown great similarities in the areas of Mondragone, Caserta and Lago Patria. On the other hand, there are some differences of the thicknesses in the Volturno Plain, where the authors suggest a thicker CI. To evaluate these discrepancies, a new proximal isopach map was drawn taking into consideration the new thickness data. The volume related to this map is 46.7 km^3, meaning a difference of 0.3 km^3 with the volume previously estimated. This value (0.3 km^3) is fully included in the 1.6 km^3 of error and uncertainties in the proximal area. For this reason, the data proposed by Ruberti et al. (2020) were not inserted

in the isopach map reported in this work, however, a greater thickness in the Volturno Plain could be considered, even though it doesn't change the final total volume of the proximal area and of all the CI.

6. The volume of the Campanian Ignimbrite

The preserved volume of the deposits of an eruption is the first essential datum to understand the magnitude of the eruption itself. These data are generally very poorly constrained for very large explosive eruptions, mainly due to the difficult to estimate the PDC volume deposits and the areal distribution of the very distal tephra layers.

The CI PDC volume was only qualitative estimated while in this work we proposed a volume calculation of the PDC deposits and consequently a more detailed determination of the CI magnitude based on the volume calculation (Mason et al., 2004).

6.1 Extracaldera volume

Our quantitative evaluation of the CI extra-caldera bulk volume (V_{pr}), is 61.5 $km^3 \pm 5.5$ km^3. However, this is not the total volume of the CI PDC deposits, which depends upon several corrections that must be applied to this value. A significant amount of pyroclastic material was deposited in the sea and within the caldera, significant erosion has occurred in the last 39.8 ka, and a large amount of co-ignimbrite ash elutriated or rose into the air as a column.

The reconstructed isopachs do not consider the linear erosion due to river incision of the CI so the possible areal erosion must be calculated. The linear erosion is referred to the selective erosion due to rivers, while the areal erosion comprises all the regional processes that occurred in the area. The deposits of WGI show a mainly valley-ponded deposit pattern; in many areas where the ignimbrite was deposited in narrow valleys (for instance near Roccamonfina), the only unit that mantles the topography is USAF, while the upper surface of WGI is mainly horizontal (Fig. 3) (Sparice, 2015). This suggests that USAF is a facies emplaced in a wider area distribution than WGI, comprising also topological highs with mantling features. The thickness of USAF is mainly between 10 cm and 1 m and, in rare cases, it can reach 3 m (L. Fedele et al., 2016). A median

thickness of 1 m is assumed as eroded material for all the enveloped area (7547 km^2, projected area) not covered by valley-pond facies, as a reference for the areal erosion. From a DEM, the real surface enveloped area was computed at 9575 km^2, meaning the calculation of the area on the DEM and not on a projected horizontal surface, it was so evaluated also the deposition on mountain slope (as a mantling feature deposition). The volume associated with the areal erosion is 9.6 km^3 (V_e) (3.7 km^3 DRE, using the average density of WGI). This is a correction based on field observation (USAF able to mantling the topography) and an average calculation (the thickness and the area), obviously, it is just a reference value, and could vary if the eroded thickness, or involved area, are considered substantially different.

The CF caldera is located near and below the current sea-level but, about 40 ka, the coastline was farther to the west and south corresponding to a level between 75 and 87 m below its present position (Antonioli, 2012; Antonioli et al., 2004; Lambeck & Bard, 2000) (Fig. 8). Based on the distribution on land of the ignimbrite, safely assumed with a radial spreading (Fisher et al., 1993; Ort et al., 2003; Thunell et al., 1979), and the position of the CF caldera relative to the coastline (Fig. 8) a roughly equal amount of material should be present both on land and offshore (Barberi et al., 1978). Flow deposits of Kos and Krakatau demonstrate that PDC can travel considerable distance above sea water (Allen & Cas, 2001; Carey et al., 1996; Dufek & Bergantz, 2007) as well the Campanian PDC flowed over the water of the Bay of Naples to deposit on the Sorrento Peninsula (~ 35 km from Pozzuoli Bay to Sorrento) (Fisher et al., 1993). As the PDC passed over the water, the more dilute upper parts did not interact with the water while the denser undercurrent developed a sheared contact with the water, leading to pyroclastic material entering the water and developing submarine currents (Dufek et al., 2007).

The presence of the turbidity currents in the Mediterranean basin and coeval to the eruption was confirmed by the analyses of the core CT85-5 in the Tyrrhenian Sea (40°19’02’’N, 11°15’42’’E) located more than 200 km west from the CF caldera (Castagnoli et al., 1995; Giaccio, 2006; Giaccio et al., 2006; Hajdas et al., 2011). The CI tephra recognized within the core was used as an important time marker and it is 45 cm thick. The nearby CT85-6 confirmed the presence of the CI tephra, however, it was less studied as its record is shorter and the CI is not reported fully (Hajdas et al., 2011). In the CI layer, were found shallow water gastropods and internal lamination, which indicate that at least 10 cm of the section are from turbiditic origin (Castagnoli et al., 1995; Giaccio, 2006; Hajdas et al., 2011). These volcanoclastic currents related to the CI eruption are

451 strongly reported in all the Tyrrhenian basin (Giaccio, 2006; McCoy & Cornell, 1990) interpreted as a large
452 syn-eruptive phenomena of the CI deposits, triggered by the PDCs which entered inside the water and in
453 general to the volcanic event. The turbidity currents can be reasonably considered as primary products of the
454 eruption (Giaccio, 2006).

455 For these reasons a large amount of underwater material is realistic and, because of the nearly equal radial area
456 covered by sea versus on land, is considered equal to the on-land material, so each is considered to have a
457 volume of 61.5 $km^3 \pm 5.5$ km^3 (V_m).

458

459 *6.2 Intracaldera volume*

460 Some deep wells were drilled in the 1940s and 1950s to understand the deep geothermal system in the Campi
461 Flegrei, reaching depths of 1600-3000 m below ground surface (Rosi & Sbrana, 1987). A well-developed
462 neogenic mineral zonation was observed with four main zones marked by distinctive mineral assemblages:
463 argillitic zone (down to ~700 m), illite-chlorite zone (down to ~1300 m), calc-aluminum silicate zone (down
464 to ~2300 m) and thermometamorphic zone (below ~2300 m). The temperatures reach high values of 360°C in
465 the calc-aluminum silicate zone (Rosi & Sbrana, 1987). These wells reached also the CI, but the extensive
466 hydrothermal alteration prevented its identification. Due to the high uncertainties of correlating CI deposits
467 inside the caldera, the isopach map was traced without the intracaldera area and the intracaldera volume was
468 not estimated in this work, which refers to literature data.

469 More recently, a 506 m drill-hole has been drilled western of Naples, reaching both NYT and CI (De Natale
470 et al., 2016; Mormone et al., 2015). The hydrothermal alteration in proximity of CI (around 439 and 501 m)
471 was recognized and made the correlation with the deposits extremely difficult. However, through lithological,
472 mineralogical and $^{40}Ar/^{39}Ar$ dating the authors recognized at least 250 m of intracaldera CI (De Natale et al.,
473 2016), this value was already observed through geological and geophysical features (Torrente et al., 2010).
474 The ignimbrite volume inside the caldera, which in this work has a dimension of 64 km^2, was then estimated
475 less than 16 km^3 (De Natale et al., 2016).

From field observation and literature data (De Natale et al., 2016), there is no evidence of significant intracaldera thickening. Therefore, a very large (~0.9) *f* value (the fraction of the total magma volume erupted prior to the onset of collapse) is attributed to the CI eruption (Cashman & Giordano, 2014). Moreover, the ratio between the measured collapses related to the NYT and CI is 2.5, a data that looks unreliable due to the much larger volume of CI than the NYT (De Natale et al., 2016). The authors proposed two models: a vent outside the Campi Flegrei caldera (model 1) and a very large regional uplift related to the CI eruption (model 2), that seems realistic to explain the anomalous ratio, especially if a much smaller eruption as Monte Nuovo one (with a volume less than 1 km^3 DRE (D'Oriano et al., 2005; Piochi et al., 2005)) produced an uplift of 5 to 8 m (Capocci, 1835; Pescandola, 1947).

There are some uncertainties due to the caldera dimension, indeed, Vitale and Isaia (2014) proposed a polygonal caldera 12 km wide, which corresponds to an area of 144 km^2. Considering an average thickness of 250 m of intracalderic deposits (De Natale et al., 2016), and an area varying from 64 to 144 km^2, the intracaldera volume (V_{intr}) ranges between 16 km^3 to 43.2 km^3 (7.9-21.4 km^3 DRE).

6.3 Distal tephra volume

The CI tephra is an important correlation tool and time marker mainly to relate the Quaternary stratigraphy in different basins and archeological sites in the Western Eurasia. The tephra layer is visible in numerous sedimentary records, including archeological (Anikovich et al., 2007; F. G. Fedele et al., 2003; Giaccio et al., 2008; Kozlowski, 1998; Pyle et al., 2006), marine (Keller et al., 1978; Paterne et al., 1986, 1999; Ton-That et al., 2001), and terrestrial sequences (Veres et al., 2013) as also cave-entrance environments (F. G. Fedele et al., 2003; Giaccio et al., 2008) and lacustrine records (Narcisi, 1996). In very distal sites, it can be found as a cryptotephra not visible to the naked eye, but clearly useful as an absolute and relative chronological and stratigraphic marker (Lowe et al., 2012). The tephra it has been identified in the Mediterranean basin (Paterne et al., 1986, 1999; Ton-That et al., 2001), in south-western Romania (Veres et al., 2013), in Italy (e.g. Monticchio, Fedele et al. 2002, 2003; Giaccio et al. 2008; Narcisi 1996), in Eastern Europe and Russia (Anikovich et al., 2007; Pyle et al., 2006), in Greece (Kozlowski, 1998), in Ukraine (Melekestev et al. 1984) and in Bulgaria (Bluszcz et al. 1992; Paterne 1992).

Define the distribution of the ultra-distal deposits is a difficult task due to the limitation of the field data available and to the thinning of the ash layers, affected by a large erosion. Underestimation of the deposit volume can be derived by simple extrapolation from proximal, medial and distal data to the ultra-distal region. Reconstructing the tephra dispersion and volume of a volcanic eruption is fundamental to understand the impact on climate, humans and ecosystems. The case of the CI is complicated by the presence of both co-plinian ash and co-ignimbrite ash due to the large-volume pyroclastic flow that generate a co-ignimbrite plume (Woods, 1998; Woods & Wohletz, 1991), both transported far away from the vent up to eastern Europe and Russia (Cornell et al., 1983; Engwell et al., 2014; F. G. Fedele et al., 2003; Giaccio et al., 2006; Narcisi & Vezzoli, 1999; Pyle et al., 2006; Smith et al., 2016; Thunell et al., 1979; Ton-That et al., 2001).

The contribution of the co-plinian and co-ignimbrite phases to the tephra layer was not an object of study in this work. However, attempt the ultra-distal tephra volume is necessary to define the total CI eruptive volume. Different authors in the past used various techniques both to define the tephra partitioning volume and to distinguish the two phases in the ash layer (Engwell et al., 2014; Marti et al., 2016; Perrotta & Scarpati, 2003; Smith et al., 2016; Sparks & Huang, 1980).

Sparks and Huang (1980) recognized the bimodal grain-size of the ultra-distal deposits of the CI, where the coarse lower unit is formed during the plinian phase, while the finer unit at the top corresponds to the co-ignimbrite phase. The authors estimated that the fine layer represents, on average, the 65% of the tephra volume, which increases away from the vent, from 20% at 450 km distance up to 95% of the deposit at 1660 km from the vent. However, an absolute volume for each phase was not defined. The decreasing of Plinian material with distance from the source was also observed by Engwell et al. (2014), who used the grain-size data to investigate the dispersal of the co-plinian and the co-ignimbrite phases. The authors calculated that 40 ± 5% of the volume of tephra within 850 km of the vent is related to the Plinian phase. Furthermore, they recognized the difficult to quantify the absolute volume of the two phases.

The first work that attributed a volume to the two components was presented by Perrotta and Scarpati (2003). The method used by the authors was previously explained. At a later time, Marti et al. (2016) modelled the CI tephra dispersion and gave a volume estimation of the two phases. They recognized the great impacts of the tephra fallout in the westward migration of modern hominid groups in Europe. Moreover, they supported the

530 hypothesis that Neanderthals populations persisted in southern Europe after the CI eruption, especially in
531 southern Iberia (Zilhão, 2006).

532 Smith et al. (2016) used the CI tephra glass composition to map the dispersal of the Plinian and the co-
533 ignimbrite components over the dispersal region. This method is substantially crucial to recognize the CI in
534 the ultra-distal region. In an especial way, it is essential to correlate this important chronological marker in
535 archeological sites and to investigate spatio-temporal variability in climate change and the timing of human
536 cultural events in eastern and central Europe (F. G. Fedele et al., 2003, 2008; L. Fedele et al., 2008; Lowe et
537 al., 2012). Based on the glass composition, the authors recognized that the PDC component is dominant in the
538 ultra-distal deposits, and the PDC produced the most voluminous deposits of the eruption.

539

540 *6.4 The volume, mass and magnitude of the CI*

541 As we said in the previous paragraph, a great part of the pyroclastic current was elutriated or rose into the air
542 as a column during the eruption and dispersed to the east (Cornell et al., 1983; Engwell et al., 2014; Perrotta
543 & Scarpati, 2003; Pyle et al., 2006; Scarpati & Perrotta, 2016; Thunell et al., 1979). The co-ignimbrite phase
544 resulted as a substantial part of the total volume; however, it remains difficult to define the associated absolute
545 volume instead of a percentage of the tephra layer.

546 The ignimbrite volume (V_i) (4 and 5) without the co-ignimbrite phase can be estimated as follows:

547 $$V_{imin} = V_{pr} + V_m + V_{intr} + 2V_e = 56 + 56 + 16 + 9.6 + 9.6 = 147.2\ km^3 \qquad \text{[Eq. 4]}$$

548 and

549 $$V_{imax} = V_{pr} + V_m + V_{intr} + 2V_e = 67 + 67 + 43.2 + 9.6 + 9.6 = 196.4\ km^3 \qquad \text{[Eq. 5]}$$

550 The total bulk PDC volume obtained by (4) and (5) is 147.2 – 196.4 km^3 (Table 3). The co-ignimbrite volume
551 (V_{ci}) is estimated using the formula (6) based on the crystal concentration method proposed by Scarpati et al.,
552 2014 (3):

553 $$V_{ci} = Vitric\ loss * V_i/(1 - Vitric\ loss) = 0.65 * V_i/(1 - 0.65) = 273.4 - 364.7\ km^3 \qquad \text{[Eq. 6]}$$

554 The co-ignimbrite volume, using a vitric loss of 0.65, ranges between 273.4 km^3 and 364.7 km^3 (107.6 km^3 –
555 143.5 km^3 DRE). However, V_{ci} could change a lot, according to the value of vitric loss used. From the
556 literature, Walker (1972) proposed for the outcrop of Altavilla (WGI), near Benevento, a vitric loss of 0.55.
557 Using this data, the co-ignimbrite bulk volume decreases and it is substantially lower between 168.2 km^3 and
558 240.0 km^3. It is necessary great attention to the right value of vitric loss to use, which can significantly influence
559 the total eruptive volume. In this work, we use 0.65, proposed by Scarpati et al. (2014), which is an average of
560 more samples located in several sites all over the CI distribution and from different units (WGI, LYT and
561 CPF). Moreover, it is not quite far from 0.55 previously proposed in literature (Walker, 1972) and the co-
562 ignimbrite volume obtained agrees with the one proposed by Costa et al. (2012) (250 - 300 km^3) using the fit
563 of an advection – diffusion tephra dispersion model to thickness data.

564 The total volume of the material erupted during the PDC phase of the CI eruption ranges between 411 km^3 and
565 561.1 km^3 (163.2 km^3 – 225.1 km^3 DRE) (Table 3). This estimate is based on the actual preserved deposits of
566 the CI so that all proposed corrections are grounded in a real starting value. Among the previous estimates
567 presented in the literature, the closest to our PDC volume are those proposed by Giaccio (2006) and Pappalardo
568 et al. (2008).

569 The fallout volume considered in this chapter is the minimum and the maximum proposed in literature by
570 Perrotta and Scarpati (2003) and Marti et al. (2016). However, no attempt is made here to evaluate or revise
571 that volume, so we do not prefer any of the previous estimates for the fallout volume and any of them could
572 be used in our total volume estimate. The total volume estimate ranges from 415 km^3 to 615.1 km^3 (164.9 km^3
573 – 247.7 km^3 DRE) (Table 3). These values are similar to some previously proposed total volumes (Cornell et
574 al., 1983; Costa et al., 2012; F. G. Fedele et al., 2003; Giaccio, 2006; Pappalardo et al., 2008; Pyle et al., 2006).
575 However, the volume proposed in this work is strictly related to the preserved volume, for the first time clearly
576 constrained by field data. The approach used in this work strongly reduces the errors and uncertainties of the
577 previous calculations.

578 The mass associated with this volume estimate is (7):

579 $$mass_{min} = 164.9\ km^3 * 2608\ kg/m^3 = 4.30 * 10^{14} kg \qquad \text{[Eq. 7]}$$

580 And (8)

$$mass_{max} = 210.7\ km^3 * 2608\ kg/m^3 = 6.46 * 10^{14} kg \quad \text{[Eq. 8]}$$

and the magnitude (M) (9) (Mason et al., 2004):

$$M\ = log10(mass) - 7 = 7.7 \quad \text{[Eq. 9]}$$

This value is consistent with a VEI 7 and a M = 7.7, which makes this eruption the largest Quaternary event from the Campi Flegrei caldera and in Europe. Our new volume estimates should help constrain the modeling of the impact on climate and the environment, including on the history of migrations of humans.

7. Conclusions

The CI eruption is the largest eruptive event of the CF caldera and a fundamental chronological marker in all central and eastern Europe. The strong impacts of this eruption on the climate induced a "volcanic winter" with a cooling effect of ~6-9°C in Eastern Europe (Black et al., 2015). The CI eruption influenced the migration of the hominid groups and it had great effects on the Paleolithic societies (Black et al., 2015; Marti et al., 2016). However, the volume of CI, fundamental to the climate impact and simulations, is poorly constrained.

Here we present a new method to trace isopachs based on the extrapolation of the paleo-topography that works well in valley-ponded ignimbrites such as the CI. A new isopach map of the extracaldera sub-aerial CI pyroclastic flow deposits yields a volume of 61.5 km^3 ± 5.5 km^3. The greater part of this volume is in the proximal area (46.4 ± 1.6 km^3, ~75%) while only around the 25% of the volume is in the distal region after the Apennines Mountain (15.1 ± 3.9 km^3).

Evidences suggest that the same amount of material should be both on land and offshore (e.g. the radial spreading of the flow). The generated submarine currents could have produced a large amount of volcanoclastic deposits in all the submarine canyons in the Gulf of Naples, as in large part of the Tyrrhenian Sea and possibly had a strong impact on the underwater dynamics of that area. Furthermore, the observation of this volcanoclastic layer can help the correlation and the understanding of sediment cores. Including separate estimates of the marine volume, the volume removed by erosion, the intracaldera volume, and the co-ignimbrite ash volume yields a total volume erupted during the PDC phase of 411.0 km^3 to 561.1 km^3 (163.2 km^3 – 225.1 km^3 DRE), values in agreement with Giaccio (2006) and Pappalardo et al. (2008).

A series of error analyses and corrections were applied to reach a total (including Plinian fallout) final volume estimate: 415.0 km^3 – 615.1 km^3 (164.9 km^3 – 247.7 km^3 DRE, in agreement with Cornell et al. (1983), Costa et al. (2012), Fedele et al. (2003), Giaccio (2006), Pappalardo et al. (2008), Pyle et al. (2006)). The volume of material, ash and aerosols is extremely important to understand and model the climate impact of this eruption, which could affect the intensity of solar radiation and consequently cause short-lived climate changes in a critical period for the modern human as the Middle to Upper Paleolithic transition.

This volume corresponds to a mass of 4.30 - 6.46 x 10^{14} kg, to a magnitude of 7.7 and to a VEI 7. This was a high impact event with significant effect on the climate and populations of the Paleolithic European region and is a proof that the Campi Flegrei caldera was able to generate a devastating eruption of this dimension.

Acknowledgments and Data

AS and GG gratefully acknowledge The Grant of Excellence Departments, MIUR-Italy. AS thanks Emanuele Sciarrino and Rose Gallo for their help in the fieldwork. We thank Danilo M. Palladino for discussions. Partial support for some field costs was provided by NSF EAR1761713 to MHO. The data presented here are available in Data Repository, online at https://mfr.osf.io/render?url=https%3A%2F%2Fosf.io%2F3a6bz%2Fdownload.

CRediT authorship contribution statement

AS: Conceptualization, Data Curation, Formal analysis, Funding acquisition, Investigation, Methodology, Validation, Visualization, Writing – Original Draft, Writing – Review & Editing. GG: Conceptualization, Funding acquisition, Methodology, Resources, Supervision, Writing – Review & Editing. RI: Resources, Supervision, Writing – Review & Editing. MHO: Funding acquisition, Writing – Review & Editing.

References

Acocella, V. (2008). Activating and reactivating pairs of nested collapses during caldera-forming eruptions: Campi Flegrei (Italy). *Geophysical Research Letters*, *35*(17), 1–5. https://doi.org/10.1029/2008GL035078

633 Albert, P. G., Giaccio, B., Isaia, R., Costa, A., Niespolo, E. M., Nomade, S., et al. (2019). Evidence for a
634 large-magnitude eruption from Campi Flegrei caldera (Italy) at 29 ka. *Geology*, *47*(7), 595–599.
635 https://doi.org/10.1130/G45805.1

636 Allen, S. R., & Cas, R. A. F. (2001). Transport of pyroclastic flows across the sea during the explosive,
637 rhyolitic eruption of the Kos Plateau Tuff, Greece. *Bulletin of Volcanology*, *62*(6–7), 441–456.
638 https://doi.org/10.1007/s004450000107

639 Anikovich, M., Sinitsyn, A. A., Hoffecker, J. F., Holliday, V. T., Popov, V. V., Lisitsyn, S. N., et al. (2007).
640 Early Upper Paleolithic in Eastern Europe and Implications for the Dispersal of Modern Humans.
641 *Science*, *315*(5809), 223–226. https://doi.org/10.1126/science.1133376

642 Antonioli, F. (2012). Sea level change in Western-Central Mediterranean since 300 kyr: Comparing global
643 sea level curves with observed data. *Alpine and Mediterranean Quaternary*, *25*(1), 15–23.

644 Antonioli, F., Bard, E., Potter, E. K., Silenzi, S., & Improta, S. (2004). 215-ka history of sea-level
645 oscillations from marine and continental layers in Argentarola Cave speleothems (Italy). *Global and*
646 *Planetary Change*, *43*(1–2), 57–78. https://doi.org/10.1016/j.gloplacha.2004.02.004

647 Barberi, F., Innocenti, F., Lirer, L., Munno, R., Pescatore, T., & Santacroce, R. (1978). The campanian
648 ignimbrite: a major prehistoric eruption in the Neapolitan area (Italy). *Bulletin Volcanologique*, *41*(1),
649 10–31. https://doi.org/10.1007/BF02597680

650 Barsotti, S., Neri, A., & Scire, J. S. (2008). The VOL-CALPUFF model for atmospheric ash dispersal: 1.
651 Approach and physical formulation. *Journal of Geophysical Research: Solid Earth*, *113*(3), 1–12.
652 https://doi.org/10.1029/2006JB004623

653 Bellucci, F. (1994). Nuove conoscenze stratigrafiche sui depositi vulcanici del sottosuolo del settore
654 meridionale della piana campana. *Boll. Soc. Geol. It.*, *113*, 395–420.

655 Black, B. A., Neely, R. R., & Manga, M. (2015). Campanian Ignimbrite volcanism, climate, and the final
656 decline of the Neanderthals. *Geology*, *43*(5), 411–414. https://doi.org/10.1130/G36514.1

657 Bonadonna, C., & Phillips, J. C. (2003). Sedimentation from strong volcanic plumes. *Journal of Geophysical*

658 *Research: Solid Earth*, *108*(B7), 1–28. https://doi.org/10.1029/2002jb002034

659 Bonadonna, C., Ernst, G. G. J., & Sparks, R. S. J. (1998). Thickness variations and volume estimates of
660 tephra fall deposits: the importance of particle Reynolds number. *Journal of Volcanology and*
661 *Geothermal Research*, *81*(3–4), 173–187. https://doi.org/10.1016/S0377-0273(98)00007-9

662 Bonadonna, C., Connor, C. B., Houghton, B. F., Connor, L., Byrne, M., Laing, A., & Hincks, T. K. (2005).
663 Probabilistic modeling of tephra dispersal: Hazard assessment of a multiphase rhyolitic eruption at
664 Tarawera, New Zealand. *Journal of Geophysical Research: Solid Earth*, *110*(3), 1–21.
665 https://doi.org/10.1029/2003JB002896

666 Bluszcz, A., Hercman, H., Pazdur, A., Pazdur, M. (1992). Radiometric dating. In *Temnata Cave.*
667 *Excavations in Karlukovo Karst Area, Bulgaria*, vol. 1.1, ed. By J.K. Kozlowski, H. Laville and B.
668 Ginter, pp. 223-240. Cracow: Jagellonian University Press.

669 Capocci, E. (1835). Nuove ricerche sul noto fenomeno delle colonne perforate dale Foladi nel tempio di
670 Serapide in Pozzuoli.

671 Cappelletti, P., Cerri, G., Colella, A., de'Gennaro, M., Langella, A., Perrotta, A., & Scarpati, C. (2003). Post-
672 eruptive processes in the Campanian Ignimbrite. *Mineralogy and Petrology*, *79*(1–2), 79–97.
673 https://doi.org/10.1007/s00710-003-0003-7

674 Carey, S., Sigurdsson, H., Mandeville, C., & Bronto, S. (1996). Pyroclastic flows and surges over water: an
675 example from the 1883 Krakatau eruption. *Bulletin of Volcanology*, *57*(7), 493–511.
676 https://doi.org/10.1007/BF00304435

677 Cashman, K. V., & Giordano, G. (2014). Calderas and magma reservoirs. *Journal of Volcanology and*
678 *Geothermal Research*, *288*, 28–45. https://doi.org/10.1016/j.jvolgeores.2014.09.007

679 Castagnoli, G. C., Albrecht, A., Beer, J., Shen, C., Callegari, E., Taricco, C., et al. (1995). Evidence for
680 enhanced 10Be deposition in Mediterranean sediments 35 Kyr BP. *Geophysical Research Letters*,
681 *22*(6), 707–710.

682 Civetta, L., Orsi, G., Pappalardo, L., Fisher, R. V., Heiken, G., & Ort, M. H. (1997). Geochemical zoning,

683 mingling, eruptive dynamics and depositional processes - the Campanian Ignimbrite, Campi Flegrei
684 caldera, Italy. *Journal of Volcanology and Geothermal Research*, *75*, 183–219.

685 Cornell, W., Carey, S., & Sigurdsson, H. (1983). Computer simulation of transport and deposition of the
686 campanian Y-5 ash. *Journal of Volcanology and Geothermal Research*, *17*(1–4), 89–109.
687 https://doi.org/10.1016/0377-0273(83)90063-X

688 Costa, A., Macedonio, G., & Folch, A. (2006). A three-dimensional Eulerian model for transport and
689 deposition of volcanic ashes. *Earth and Planetary Science Letters*, *241*(3–4), 634–647.
690 https://doi.org/10.1016/j.epsl.2005.11.019

691 Costa, A., Folch, A., Macedonio, G., Giaccio, B., Isaia, R., & Smith, V. C. (2012). Quantifying volcanic ash
692 dispersal and impact of the Campanian Ignimbrite super-eruption. *Geophysical Research Letters*,
693 *39*(10), 3–7. https://doi.org/10.1029/2012GL051605

694 Costa, A., Suzuki, Y. J., & Koyaguchi, T. (2018). Understanding the plume dynamics of explosive super-
695 eruptions. *Nature Communications*, *9*(1). https://doi.org/10.1038/s41467-018-02901-0

696 De Natale, G., Troise, C., Mark, D., Mormone, A., Piochi, M., Di Vito, M. A., et al. (2016). The Campi
697 Flegrei Deep Drilling Project (CFDDP): New insight on caldera structure, evolution and hazard
698 implications for the Naples area (Southern Italy). *Geochemistry Geophysics Geosystems*, *17*, 2825–
699 2834. https://doi.org/10.1002/2016GC006406

700 De Vivo, B., Rolandi, G., Gans, P. B., Calvert, A., Bohrson, W. A., Spera, F. J., & Belkin, H. E. (2001). New
701 constraints on the pyroclastic eruptive history of the Campanian volcanic Plain (Italy). *Mineralogy and*
702 *Petrology*, *73*(1–3), 47–65. https://doi.org/10.1007/s007100170010

703 Di Vito, M. A., Isaia, R., Orsi, G., Southon, J., De Vita, S., D'Antonio, M., et al. (1999). Volcanism and
704 deformation since 12,000 years at the Campi Flegrei caldera (Italy). *Journal of Volcanology and*
705 *Geothermal Research*, *91*(2–4), 221–246. https://doi.org/10.1016/S0377-0273(99)00037-2

706 D'Oriano, C., Poggianti, E., Bertagnini, A., Cioni, R., Landi, P., Polacci, M., & Rosi, M. (2005). Changes in
707 eruptive style during the A.D. 1538 Monte Nuovo eruption (Phlegrean Fields, Italy): The role of syn-
708 eruptive crystallization. *Bulletin of Volcanology*, *67*(7), 601–621. https://doi.org/10.1007/s00445-004-

0397-z

Dufek, J., & Bergantz, G. W. (2007). Dynamics and deposits generated by the Kos Plateau Tuff eruption: Controls of basal particle loss on pyroclastic flow transport. *Geochemistry, Geophysics, Geosystems*, *8*(12). https://doi.org/10.1029/2007GC001741

Dufek, J., Manga, M., & Staedter, M. (2007). Littoral blasts: Pumice-water heat transfer and the conditions for steam explosions when pyroclastic flows enter the ocean. *Journal of Geophysical Research: Solid Earth*, *112*(11), 1–16. https://doi.org/10.1029/2006JB004910

Engwell, S., Sparks, R. S. J., & Carey, S. (2014). Physical characteristics of tephra layers in the deep sea realm: the Campanian Ignimbrite eruption. *Geological Society, London, Special Publications*, *398*(1), 47–64. https://doi.org/10.1144/SP398.7

Fedele, F. G., Giaccio, B., Isaia, R., & Orsi, G. (2002). Ecosystem Impact of the Campanian Ignimbrite Eruption in Late Pleistocene Europe. *Quaternary Research*, *57*(3), 420–424. https://doi.org/10.1006/qres.2002.2331

Fedele, F. G., Giaccio, B., Isaia, R., & Orsi, G. (2003). The Campanian ignimbrite eruption, Heinrich event 4, and Palaeolithic change in Europe: a high-resolution investigation. *Geophysical Monograph*, 301–325. https://doi.org/10.1029/139GM20

Fedele, F. G., Giaccio, B., Isaia, R., Orsi, G., Carroll, M. R., & Scaillet, B. (2007). The Campanian Ignimbrite Factor: Towards a Reappraisal of the Middle to Upper Palaeolithic "Transition." *Living Under The Shadow. Cultural Impacts of Volcanic Eruptions*, 19–41.

Fedele, F. G., Giaccio, B., & Hajdas, I. (2008). Timescales and cultural process at 40,000 BP in the light of the Campanian Ignimbrite eruption, Western Eurasia. *Journal of Human Evolution*, *55*(5), 834–857. https://doi.org/10.1016/j.jhevol.2008.08.012

Fedele, L., Scarpati, C., Lanphere, M., Melluso, L., Morra, V., Perrotta, A., & Ricci, G. (2008). The Breccia Museo formation, Campi Flegrei, southern Italy: Geochronology, chemostratigraphy and relationship with the Campanian Ignimbrite eruption. *Bulletin of Volcanology*, *70*(10), 1189–1219. https://doi.org/10.1007/s00445-008-0197-y

735 Fedele, L., Scarpati, C., Sparice, D., Perrotta, A., & Laiena, F. (2016). A chemostratigraphic study of the
736 Campanian Ignimbrite eruption (Campi Flegrei, Italy): Insights on magma chamber withdrawal and
737 deposit accumulation as revealed by compositionally zoned stratigraphic and facies framework. *Journal*
738 *of Volcanology and Geothermal Research*, *324*, 105–117.
739 https://doi.org/10.1016/j.jvolgeores.2016.05.019

740 Fisher, R. V., Orsi, G., Ort, M. H., & Heiken, G. (1993). Mobility of a large-volume pyroclastic flow -
741 emplacement of the Campanian ignimbrite, Italy. *Journal of Volcanology and Geothermal Research*,
742 *56*(3), 205–220. https://doi.org/10.1016/0377-0273(93)90017-L

743 Folch, A. (2012). A review of tephra transport and dispersal models: Evolution, current status, and future
744 perspectives. *Journal of Volcanology and Geothermal Research*, *235–236*, 96–115.
745 https://doi.org/10.1016/j.jvolgeores.2012.05.020

746 Folch, A., Costa, A., Durant, A., & Macedonio, G. (2010). A model for wet aggregation of ash particles in
747 volcanic plumes and clouds: 2. Model application. *Journal of Geophysical Research: Solid Earth*,
748 *115*(9), 1–16. https://doi.org/10.1029/2009JB007176

749 Giaccio, B. (2006). *L'eruzione dell'Ignimbrite Campana (c . 40 ka BP), oscillazioni climatiche sub-orbitali e*
750 *i cambiamenti bioculturali dell'OIS 3 europeo*. Università degli Studi di Napoli "Federico II."

751 Giaccio, B., Hajdas, I., Peresani, M., Fedele, F. G., & Isaia, R. (2006). The Campanian Ignimbrite tephra and
752 its relevnce for the timing of the middle to upper paleolithic shift. In *When Neanderthals and modern*
753 *humans met* (pp. 343–375).

754 Giaccio, B., Isaia, R., Fedele, F. G., Di Canzio, E., Hoffecker, J. F., Ronchitelli, A., et al. (2008). The
755 Campanian Ignimbrite and Codola tephra layers: Two temporal/stratigraphic markers for the Early
756 Upper Palaeolithic in southern Italy and eastern Europe. *Journal of Volcanology and Geothermal*
757 *Research*, *177*(1), 208–226. https://doi.org/10.1016/j.jvolgeores.2007.10.007

758 Giaccio, B., Hajdas, I., Isaia, R., Deino, A. L., & Nomade, S. (2017). dating of the Campanian Ignimbrite (
759 Y-5) reconciles the time-scales of climatic-cultural processes at 40 ka. *Nature Publishing Group*,
760 (January), 1–10. https://doi.org/10.1038/srep45940

761 Hajdas, I., Taricco, C., Bonani, G., Beer, J., Bernasconi, S. M., & Wacker, L. (2011). Anomalous
762 radiocarbon ages found in Campanian Ignimbrite deposit of the Mediterranean deep-sea core CT85-5.
763 *Radiocarbon*, *53*(4), 575–583.

764 Isaia, R., Marianelli, P., & Sbrana, A. (2009). Caldera unrest prior to intense volcanism in Campi Flegrei
765 (Italy) at 4.0 ka B.P.: Implications for caldera dynamics and future eruptive scenarios. *Geophysical*
766 *Research Letters*, *36*(21), 1–6. https://doi.org/10.1029/2009GL040513

767 ISPRA (2009). Geological Map n. 432 ‘‘Benevento’’; scale 1:50,000. *National Geological Survey of Italy*,
768 Università degli studi di Urbino, Istituto di Geologia Applicata, Urbino, Italy.

769 ISPRA (2010). Geological Map n. 431 ‘‘Caserta Est’’; scale 1:50,000. *National Geological Survey of Italy*,
770 Regione Campania, Settore Difesa Suolo, Napoli, Italy.

771 ISPRA (2011a). Geological Map n. 465 ‘‘Isola di Procida’’; scale 1:50,000. *National Geological Survey of*
772 *Italy*, Regione Campania, Settore Difesa Suolo, Napoli, Italy.

773 ISPRA (2011b). Geological Map n. 448 ‘‘Ercolano’’; scale 1:50,000. *National Geological Survey of Italy*,
774 CNR Consiglio Nazionale delle Ricerche, Italy.

775 ISPRA (2011c). Geological Map n. 467 ‘‘Salerno’’; scale 1:50,000. *National Geological Survey of Italy*,
776 (http://www.isprambiente.gov.it/MEDIA/carg/ campania.html).

777 ISPRA (2011d). Geological Map n. 446-447 ‘‘Napoli’’; scale 1:50,000. *National Geological Survey of Italy*,
778 Regione Campania - Settore Difesa Suolo, Napoli, Italy.

779 ISPRA (2014°). Geological Map n. 450 ‘‘S.Angelo dei Lombardi’’; scale 1:50,000. *National Geological*
780 *Survey of Italy*, CNR Consiglio Nazionale delle Ricerche, Italy.

781 ISPRA (2014b). Geological Map n. 466-485 ‘‘Sorrento-Termini’’; scale 1:50,000. *National Geological*
782 *Survey of Italy*, CNR Consiglio Nazionale delle Ricerche, Italy.

783 ISPRA (2016). Geological Map n. 449 ‘‘Avellino’’; scale 1:50,000. *National Geological Survey of Italy*,
784 Regione Campania, Italy.

785 ISPRA (2018). Geological Map n. 464 ‘‘Isola d’Ischia’’; scale 1:25,000. *National Geological Survey of Italy*,

786 Regione Campania, Settore Difesa Suolo, Napoli, Italy.

787 Keller, J., Ryan, W. B. F., Ninkovich, D., & Altherr, R. (1978). Explosive volcanic activity in the
788 Mediterranean over the past 200,000 yr as recorded in deep-sea sediments. *Bulletin of the Geological*
789 *Society of America*, *89*(4), 591–604. https://doi.org/10.1130/0016-
790 7606(1978)89<591:EVAITM>2.0.CO;2

791 Kozlowski, J. K. (1998). The Middle and the Early Upper Paleolithic around the black sea. In *Neandertals*
792 *and Modern Humans in Western Asia* (pp. 461–482). New York: Plenum Press.

793 Lambeck, K., & Bard, E. (2000). Sea-level change along the French Mediterranean coast for the past 30000
794 years. *Earth and Planetary Science Letters*, *175*(3–4), 203–222.

795 Langella, A., Bish, D. L., Calcaterra, D., & Cappelletti, P. (2013). L'Ignimbrite Campana (IC). In L. Editore
796 (Ed.), *Le pietre storiche della Campania dall'oblio alla riscoperta* (pp. 155–177).

797 Lowe, J., Barton, N., Blockley, S., Ramsey, C. B., Cullen, V. L., Davies, W., et al. (2012). Volcanic ash
798 layers illuminate the resilience of Neanderthals and early modern humans to natural hazards.
799 *Proceedings of the National Academy of Sciences*, *109*(34), 13532–13537.
800 https://doi.org/10.1073/pnas.1204579109

801 Marianelli, P., Sbrana, A., & Proto, M. (2006). Magma chamber of the Campi Flegrei supervolcano at the
802 time of eruption of the Campanian Ignimbrite. *Geology*, *34*(11), 937–940.
803 https://doi.org/10.1130/G22807A.1

804 Marti, A., Folch, A., Costa, A., & Engwell, S. (2016). Reconstructing the plinian and co-ignimbrite sources
805 of large volcanic eruptions: A novel approach for the Campanian Ignimbrite. *Scientific Reports*, *6*(1),
806 21220. https://doi.org/10.1038/srep21220

807 Mason, B. G., Pyle, D. M., & Oppenheimer, C. (2004). The size and frequency of the largest explosive
808 eruptions on Earth. *Bulletin of Volcanology*, *66*(8), 735–748. https://doi.org/10.1007/s00445-004-0355-
809 9

810 McCoy, F.W., & Cornell, W. (1990). Volcaniclastic sediments in the Tyrrhenian basin. In K.A. Kastens and

J. Mascle et al. (eds.) "*Proceedings of the ODP*", 291-305. Scientific Results 107.

Melekestsev, I.V., Kirianov, V.Y., & Praslov, N.D. (1984). Catastrophic eruption in the Phlegrean Fields region (Italy) - possible source for a volcanic ash in late Pleistocene sediments of the European part of the USSR. *Vulcanologija i Seismologija* 3, 35-44.

Melluso, L., Morra, V., Perrotta, A., Scarpati, C., & Adabbo, M. (1995). The eruption of the Breccia Museo (Campi Flegrei, Italy): Fractional crystallization processes in a shallow, zoned magma chamber and implications for the eruptive dynamics. *Journal of Volcanology and Geothermal Research*, *68*(4), 325–339. https://doi.org/10.1016/0377-0273(95)00020-5

Milia, A., & Torrente, M. M. (2007). The influence of paleogeographic setting and crustal subsidence on the architecture of ignimbrites in the Bay of Naples (Italy). *Earth and Planetary Science Letters*, *263*, 192–206. https://doi.org/10.1016/j.epsl.2007.08.004

Mormone, A., Troise, C., Piochi, M., Balassone, G., Joachimski, M., & De Natale, G. (2015). Mineralogical, geochemical and isotopic features of tuffs from the CFDDP drill hole: Hydrothermal activity in the eastern side of the Campi Flegrei volcano (southern Italy). *Journal of Volcanology and Geothermal Research*, *290*, 39–52. https://doi.org/10.1016/j.jvolgeores.2014.12.003

Narcisi, B. (1996). Tephrochronology of a late quaternary lacustrine record from the Monticchio maar (Vulture volcano, southern Italy). *Quaternary Science Reviews*, *15*(2–3), 155–165. https://doi.org/10.1016/0277-3791(95)00045-3

Narcisi, B., & Vezzoli, L. (1999). Quaternary stratigraphy of distal tephra layers in the Mediterranean - An overview. *Global and Planetary Change*, *21*(1–3), 31–50. https://doi.org/10.1016/S0921-8181(99)00006-5

Orsi, G., De Vita, S., & Di Vito, M. A. (1996). The restless, resurgent Campi Flegrei nested caldera (Italy): constraints on its evolution and configuration. *Journal of Volcanology and Geothermal Research*, *74*, 179–214.

Ort, M. H., Orsi, G., Pappalardo, L., & Fisher, R. V. (2003). Anisotropy of magnetic susceptibility studies of depositional processes in the Campanian Ignimbrite , Italy. *Bulletin of Volcanology*, *65*, 55–72.

837 https://doi.org/10.1007/s00445-002-0241-2

838 Ortolani, F., & Aprile, F. (1985). Principali caratteristiche stratigrafiche e strutturali dei depositi superficiali
839 della piana campana. *Boll. Soc. Geol. It.*, *104*, 195–206.

840 Pappalardo, L., Civetta, L., D'Antonio, M., Deino, A. L., Di Vito, M. A., Orsi, G., et al. (1999). Chemical
841 and Sr-isotopical evolution of the Phlegraean magmatic system before the Campanian Ignimbrite and
842 the Neapolitan Yellow Tuff eruptions. *Journal of Volcanology and Geothermal Research*, *91*(2–4),
843 141–166. https://doi.org/10.1016/S0377-0273(99)00033-5

844 Pappalardo, L., Ottolini, L., & Mastrolorenzo, G. (2008). The Campanian Ignimbrite (southern Italy)
845 geochemical zoning: Insight on the generation of a super-eruption from catastrophic differentiation and
846 fast withdrawal. *Contributions to Mineralogy and Petrology*, *156*(1), 1–26.
847 https://doi.org/10.1007/s00410-007-0270-0

848 Parfitt, L., & Wilson, L. (2008). Fundamentals of Physical Volcanology. Blackwell, Malden, USA (256 pp.).

849 Paterne, M. (1992). Additional remarks on tephra layer from Temnata Cave, in *Temnata Cave. Excavations*
850 *in Karlukovo Karst area, Bulgaria*, edited by J.K. Kozlowski, H. Laville and B. Ginter, pp. 99-100,
851 Jagellonian University Press, Cracow.

852 Paterne, M., Guichard, F., Labeyrie, J., Gillot, P. Y., & Duplessy, J. C. (1986). Tyrrhenian Sea
853 tephrochronology of the oxygen isotope record for the past 60,000 years. *Marine Geology*, *72*(3–4),
854 259–285. https://doi.org/10.1016/0025-3227(86)90123-4

855 Paterne, M., Kallel, N., Labeyrie, L., Vautravers, M., Duplessy, J. C., Rossignol-Strick, M., et al. (1999).
856 Hydrological relationship between the North Atlantic Ocean and the Mediterranean Sea during the past
857 15 - 75 kyr. *Paleoceanography*, *14*(5), 626–638. https://doi.org/10.1029/1998PA900022

858 Perrotta, A., & Scarpati, C. (1994). The dynamics of the Breccia Museo eruption (Campi Flegrei, Italy) and
859 the significance of spatter clasts associated with lithic breccias. *Journal of Volcanology and*
860 *Geothermal Research*, *59*(4), 335–355. https://doi.org/10.1016/0377-0273(94)90086-8

861 Perrotta, A., & Scarpati, C. (2003). Volume partition between the plinian and co-ignimbrite air fall deposits

of the Campanian Ignimbrite eruption. *Mineralogy and Petrology*, *79*(1–2), 67–78. https://doi.org/10.1007/s00710-003-0002-8

Perrotta, A., Scarpati, C., Luongo, G., & Morra, V. (2006). Chapter 5 The Campi Flegrei caldera boundary in the city of Naples. *Developments in Volcanology*, *9*(C), 85–96. https://doi.org/10.1016/S1871-644X(06)80019-7

Perrotta, A., Scarpati, C., Luongo, G., & Morra, V. (2010). Stratigraphy and volcanological evolution of the southwestern sector of Campi Flegrei and Procida Island , Italy. *The Geological Society of America Special Paper*, *80301*(303), 171–191. https://doi.org/10.1130/2010.2464(09).

Piochi, M., Mastrolorenzo, G., & Pappalardo, L. (2005). Magma ascent and eruptive processes from textural and compositional features of Monte Nuovo pyroclastic products, Campi Flegrei, Italy. *Bulletin of Volcanology*, *67*(7), 663–678. https://doi.org/10.1007/s00445-005-0410-1

Pyle, D.M. (1990). New volume estimates for the Minoan eruption of Santorini. In: Hardy, D.A., Keller, J., Galanopoulos, V., Flemming, N.C., Druitt, T.H. (Eds.), *Thera and the Aegean World III*, The Thera Foundation, London, vol. 2, pp. 113–121

Pyle, D. M. (1989). The thickness, volume and grainsize of tephra fall deposits. *Bulletin of Volcanology*, *51*, 1–15.

Pyle, D. M., Ricketts, G. D., Margari, V., van Andel, T. H., Sinitsyn, A. A., Praslov, N. D., & Lisitsyn, S. N. (2006). Wide dispersal and deposition of distal tephra during the Pleistocene "Campanian Ignimbrite/Y5" eruption, Italy. *Quaternary Science Reviews*, *25*(21–22), 2713–2728. https://doi.org/10.1016/j.quascirev.2006.06.008

Rampino, M. R., & Self, S. (1992). Volcanic winter and accelerated glaciation following the Toba super-eruption. *Nature*, *359*, 50–52.

Rolandi, G., Bellucci, F., Heizler, M. T., Belkin, H. E., & De Vivo, B. (2003). Tectonic controls on the genesis of ignimbrites from the Campanian Volcanic Zone, southern Italy. *Mineralogy and Petrology*, *79*(1–2), 3–31. https://doi.org/10.1007/s00710-003-0014-4

887 Rosi, M., Sbrana, A. (1987). Phlegrean Fields. CNR, *Quaderni de La ''Ricerca Scientifica''* 114, 1–175.

888 Rosi, M., Sbrana, A., & Principe, C. (1983). The phlegraean fields: Structural evolution, volcanic history and
889 eruptive mechanisms. *Journal of Volcanology and Geothermal Research*, *17*(1–4), 273–288.
890 https://doi.org/10.1016/0377-0273(83)90072-0

891 Rosi, M., Sbrana, A., & Vezzoli, L. (1988). Correlazioni tefrostratigrafiche di alcuni livelli di Ischia, Procida
892 e Campi Flegrei. *Memorie Della Società Geologica Italiana*, *41*, 1015–1027.

893 Rosi, M., Vezzoli, L., Aleotti, P., & Censi, M. (1996). Interaction between caldera collapse and eruptive
894 dynamics during the Campanian Ignimbrite eruption, Phlegraean Fields, Italy. *Bulletin of Volcanology*,
895 *57*(7), 541–554. https://doi.org/10.1007/BF00304438

896 Rosi, M., Vezzoli, L., Castelmenzano, A., & Grieco, G. (1999). Plinian pumice fall deposit of the Campanian
897 Ignimbrite eruption (Phlegraean Fields, Italy). *Journal of Volcanology and Geothermal Research*,
898 *91*(2–4), 179–198. https://doi.org/10.1016/S0377-0273(99)00035-9

899 Ruberti, D., Vigliotti, M., Rolandi, R., & Lascio, M. Di. (2020). Effect of paleomorphology on facies
900 distribution of the Campania Ignimbrite in the northern Campania Plain, southern Italy. In *Vesuvius,*
901 *Campi Flegrei, and Campanian Volcanism* (pp. 207–229). Elsevier Inc. https://doi.org/10.1016/B978-
902 0-12-816454-9.00009-2

903 Sbrana, A., Toccaceli, R. M. (2011). Carta Geologica della Regione Campania in scala 1: 10.000, Foglio 464
904 Isola d'Ischia.

905 Scandone, R., Bellucci, F., Lirer, L., & Rolandi, G. (1991). The structure of the Campanian Plain and the
906 activity of the Neapolitan volcanoes (Italy). *Journal of Volcanology and Geothermal Research*, *48*(1–
907 2), 1–31. https://doi.org/10.1016/0377-0273(91)90030-4

908 Scarpati, C., & Perrotta, A. (2012). Erosional characteristics and behavior of large pyroclastic density
909 currents. *Geology*, *40*(11), 1035–1038. https://doi.org/10.1130/G33380.1

910 Scarpati, C., & Perrotta, A. (2016). Stratigraphy and physical parameters of the Plinian phase of the
911 Campanian Ignimbrite eruption. *Bulletin of the Geological Society of America*, *128*(7), 1147–1159.

912 https://doi.org/10.1130/B31331.1

913 Scarpati, C., Perrotta, A., Lepore, S., & Calvert, A. (2013). Eruptive history of Neapolitan volcanoes :
914 constraints from 40 Ar – 39 Ar dating. *Geological Magazine*, *150*(3), 412–425.
915 https://doi.org/10.1017/S0016756812000854

916 Scarpati, C., Sparice, D., & Perrotta, A. (2014). A crystal concentration method for calculating ignimbrite
917 volume from distal ash-fall deposits and a reappraisal of the magnitude of the Campanian Ignimbrite.
918 *Journal of Volcanology and Geothermal Research*, *280*, 67–75.
919 https://doi.org/10.1016/j.jvolgeores.2014.05.009

920 Scarpati, C., Sparice, D., & Perrotta, A. (2015a). Facies variation in the Campanian Ignimbrite. *Rendiconti*
921 *Online Societa Geologica Italiana*, *33*, 83–87. https://doi.org/10.3301/ROL:2015.20

922 Scarpati, C., Sparice, D., & Perrotta, A. (2015b). The ground layer of the Campanian Ignimbrite: an example
923 of deposition from a dilute pyroclastic density current. *Bulletin of Volcanology*, *77*(11).
924 https://doi.org/10.1007/s00445-015-0985-0

925 Servizio Geologico d'Italia (1963). Carta geologica d'Italia scala 1:100.000, foglio 174 – Ariano Irpino
926 "*Geological map of Italy at 1:100.000 scale, sheet number 174 – Ariano Irpino*". Servizio Geologico
927 d'Italia, Rome.

928 Servizio Geologico d'Italia (1965a). Carta geologica d'Italia scala 1:100.000, foglio 185 – Salerno
929 "*Geological map of Italy at 1:100.000 scale, sheet number 185 – Salerno*". Servizio Geologico d'Italia,
930 Rome.

931 Servizio Geologico d'Italia (1965b). Carta geologica d'Italia scala 1:100.000, foglio 196 – Sorrento
932 "*Geological map of Italy at 1:100.000 scale, sheet number 196 – Sorrento*". Servizio Geologico
933 d'Italia, Rome.

934 Servizio Geologico d'Italia (1965c). Carta geologica d'Italia scala 1:100.000, foglio 197 – Amalfi
935 "*Geological map of Italy at 1:100.000 scale, sheet number 197 – Amalfi*". Servizio Geologico d'Italia,
936 Rome.

Servizio Geologico d'Italia (1966). Foglio Geologico n°172 - Caserta. *Carta Geologica d'Italia, scala 1:100.000*, II ediz., Istituto Poligrafico e Zecca dello Stato, Roma.

Servizio Geologico d'Italia (1967a). Carta geologica d'Italia scala 1:100.000, fogli 183-184 – Isola di Ischia – Napoli "*Geological map of Italy at 1:100.000 scale, sheet number 183-184 – Isola di Ischia - Napoli*". Servizio Geologico d'Italia, Rome.

Servizio Geologico d'Italia (1967b). Carta geologica d'Italia scala 1:100.000, fogli 160 – Cassino "*Geological map of Italy at 1:100.000 scale, sheet number 160 – Cassino*". Servizio Geologico d'Italia, Rome.

Servizio Geologico d'Italia (1971a). Carta geologica d'Italia scala 1:100.000, foglio 171 – Gaeta e Vulcano di Roccamonfina "*Geological map of Italy at 1:100.000 scale, sheet number 171 – Gaeta e Vulcano di Roccamonfina*". Servizio Geologico d'Italia, Rome.

Servizio Geologico d'Italia (1971b). Carta geologica d'Italia scala 1:100.000, foglio 161 – Isernia "*Geological map of Italy at 1:100.000 scale, sheet number 161 – Isernia*". Servizio Geologico d'Italia, Rome.

Servizio Geologico d'Italia (1975). Carta geologica d'Italia scala 1:100.000, foglio 173 – Benevento "*Geological map of Italy at 1:100.000 scale, sheet number 173 – Benevento*". Servizio Geologico d'Italia, Rome.

Seymour, K., & Christanis, K. (1995). Correlation of a tephra layer in western greece with a late pleistocene eruption in the campanian province of italy. *Quaternary Research*. https://doi.org/10.1006/qres.1995.1005

Seymour, K. S., Christanis, K., Bouzinos, A., Papazisimou, S., Papatheodorou, G., Moran, E., & Dénès, G. (2004). Tephrostratigraphy and tephrochronology in the Philippi peat basin, Macedonia, Northern Hellas (Greece). *Quaternary International*, *121*(1), 53–65. https://doi.org/10.1016/j.quaint.2004.01.023

Smith, V. C., Isaia, R., & Pearce, N. J. G. (2011). Tephrostratigraphy and glass compositions of post-15 kyr Campi Flegrei eruptions: Implications for eruption history and chronostratigraphic markers. *Quaternary Science Reviews*, *30*(25–26), 3638–3660. https://doi.org/10.1016/j.quascirev.2011.07.012

963 Smith, V. C., Isaia, R., Engwell, S., & Albert, P. G. (2016). Tephra dispersal during the Campanian
964 Ignimbrite (Italy) eruption: implications for ultra-distal ash transport during the large caldera-forming
965 eruption. *Bulletin of Volcanology*, *78*(6). https://doi.org/10.1007/s00445-016-1037-0

966 Sparice, D. (2015). *Definizione delle litofacies e ricostruzione dell'architettura dell'Ignimbrite Campana*.
967 Università degli Studi di Napoli Federico II.

968 Sparks, R. S. J., & Huang, T. C. (1980). The volcanological significance of deep-sea ash layer associated
969 with ignimbrites. *Geological Magazine*, *117*(5), 425–436.

970 Sparks, S., Self, S., Grattan, J., Oppenheimer, C., Pyle, D., Rymer, H. (2005). Super- eruptions: global
971 effects and future threats, *Report of a Geological Society of London Working Group*, (2nd (print)
972 Edition).

973 Sparks, R. S. J., & Walker, G. P. L. (1977). The significance of vitric-enriched air-fall ashes associated with
974 crystal-enriched ignimbrites. *Journal of Volcanology and Geothermal Research*, *2*, 329–341.

975 Stuiver, M., Grootes, P. M., & Braziunas, T. F. (1995). The GISP2 □18O Climate Record of the Past 16,500
976 Years and the Role of the Sun, Ocean, and Volcanoes. *Quaternary Research*, *44*, 341–354.

977 Tanguy, J. C., Ribière, C., Scarth, A., & Tjetjep, W. S. (1998). Victims from volcanic eruptions: a revised
978 database. *Bulletin of Volcanology*, *60*(2), 137–144. https://doi.org/10.1007/s004450050222

979 Thordarson, T., & Self, S. (1996). Sulfur, chlorine and fluorine degassing and atmospheric loading by the
980 Roza eruption, Columbia River Basalt Group, Washington, USA. *Journal of Volcanology and*
981 *Geothermal Research*, *74*, 49–73.

982 Thunell, R., Federman, A., Sparks, R. S. J., & Williams, D. (1979). The age, origin, and volcanological
983 significance of the Y-5 ash layer in the Mediterranean. *Quaternary Research*, *12*(2), 241–253.
984 https://doi.org/10.1016/0033-5894(79)90060-7

985 Ton-That, T., Singer, B., & Paterne, M. (2001). 40Ar/39 dating of latest Pleistocene (41 ka) marine tephra in
986 the Mediterranean sea: Implications for global climate records. *Earth and Planetary Science Letters*,
987 *184*(3–4), 645–658. https://doi.org/10.1016/S0012-821X(00)00358-7

988 Torrente, M. M., Milia, A., Bellucci, F., & Rolandi, G. (2010). Extensional tectonics in the Campania
989 Volcanic Zone (eastern Tyrrhenian Sea , Italy): New insights into the relationship between faulting
990 and ignimbrite eruptions. *Boll. Soc. Geol. It.*, *129*, 297–315. https://doi.org/10.3301/IJG.2010.07

991 Upton, J., Cole, P., Shaw, P., Szakacs, A., Seghedi, I. (2002). Correlation of tephra layers found in southern
992 Romania with the Campanian Ignimbrite (~37 ka) eruption. In: *The Quaternary Research Association*
993 *and First Postgraduate Paleo-environmental Symposium*, 36. Amsterdam: Universiteit van Amsterdam.

994 Veres, D., Lane, C. S., Timar-Gabor, A., Hambach, U., Constantin, D., Szakács, A., et al. (2013). The
995 Campanian Ignimbrite/Y5 tephra layer - A regional stratigraphic marker for Isotope Stage 3 deposits in
996 the Lower Danube region, Romania. *Quaternary International*, *293*, 22–33.
997 https://doi.org/10.1016/j.quaint.2012.02.042

998 Vezzoli, L., Barberi, F. (1988). Progetto finalizzato geodinamica: monografie finali. X: Island of Ischia.
999 *Quaderni de La ricerca scientifica*, (114).

1000 Vitale, S., & Isaia, R. (2014). Fractures and faults in volcanic rocks (Campi Flegrei, southern Italy): Insight
1001 into volcano-tectonic processes. *International Journal of Earth Sciences*, *103*(3), 801–819.
1002 https://doi.org/10.1007/s00531-013-0979-0

1003 Walker, G. P. L. (1972). Crystal concentration in ignimbrites. *Contributions to Mineralogy and Petrology*,
1004 *36*(2), 135–146. https://doi.org/10.1007/BF00371184

1005 Walker, G. P. L. (1980). The Taupo pumice: product of the most powerful known (ultraplinian) eruption?
1006 *Journal of Volcanology and Geothermal Research*, *8*, 69–94.

1007 Walker, G. P. L. (1981). Characteristics of two phreatoplinian ashes, and their water-flushed origin. *Journal*
1008 *of Volcanology and Geothermal Research*, *9*(4), 395–407. https://doi.org/10.1016/0377-
1009 0273(81)90046-9

1010 Wilson, C. J. N., & Walker, G. P. L. (1985). The Taupo eruption, New Zealand. 1. General aspects.
1011 *Philosophical Transactions of the Royal Society A: Mathematical, Physical and Engineering Sciences*,
1012 *314*(1529), 199–228.

1013 Witham, C. S. (2005). Volcanic disasters and incidents: A new database. *Journal of Volcanology and*
1014 *Geothermal Research*, *148*(3–4), 191–233. https://doi.org/10.1016/j.jvolgeores.2005.04.017

1015 Woods, A. W. (1998). Observations and models of volcanic eruption columns. *Geological Society Special*
1016 *Publication*, *145*, 91–114. https://doi.org/10.1144/GSL.SP.1996.145.01.06

1017 Woods, A. W., & Wohletz, K. (1991). Dimensions and dynamics of co-ignimbrite eruption columns. *Nature*,
1018 *350*(6315), 225–227. https://doi.org/10.1038/350225a0

1019 Zilhão, J. (2006). Neandertals and moderns mixed, and it matters. *Evolutionary Anthropology*, *15*(5), 183–
1020 195. https://doi.org/10.1002/evan.20110

1021

Tables

	Volume calculations (km^3)					
Authors	Plinian fallout	Co-plinian ash	PDC	Co-ignimbrite ash	Y-5	Total
Thunell et al., 1979			30-40*		30-40*	60-80*
Cornell et al., 1983					73	>150
Fisher et al., 1993			500			
Civetta et al., 1997	25*		120*			145*
Rosi et al., 1999	15					
Fedele et al., 2003						200*
Perrotta and Scarpati, 2003	4	16		100 (42*)		
Rolandi et al., 2003			180	140		320 (200*)
Giaccio, 2006	10 (3*)		385 (215*)	180 (86*)		575 (300*)
Marianelli et al., 2006	20*		130*			150*
Pyle et al., 2006				72-120 (31-50*)		105-210*
Pappalardo et al., 2008	20*		180*			200*
Costa et al., 2012				250-300 (104-125*)		430-680 (180-280*)
Scarpati et al., 2014			54 (25*)	100 (42*)		
Marti et al., 2016	54 (22.6*)			153.9 (61.6*)		207.9 (84.2*)
Scarpati and Perrotta, 2016	5.33 (0.88*)	14.67 (6.88*)				

Table 1*. Bulk and DRE (*) volume calculations proposed for the CI by different authors, in approximate chronological order. Y-5 refers to those studies that did not identify the co-plinian and co-ignimbrite contribution. The methods are described in the text.*

Thickness (km)	**Area (m^2)**	**Area (km^2)**	**Cumulative area (km^2)**	**Volume (km^3)**	**Cumulative Volume (km^3)**	**Volume (%)**
0.08	12613584.05	12.61	12.61	0.19	0.19	0.33
0.07	12329142.98	12.33	24.94	0.16	0.35	0.28
0.06	19116655.52	19.12	44.06	0.25	0.60	0.44
0.05	31312007.72	31.31	75.37	1.33	1.92	2.34
0.04	234023868.7	234.02	309.40	2.14	4.07	3.78
0.03	194514229.9	194.51	503.91	5.24	9.31	9.24
0.02	853977772.9	853.98	1357.89	8.58	17.89	15.13
0.01	862025846	862.03	2219.91	9.29	27.18	16.38
0		995.70	3215.61	34.32	**61.50**	60.52

Table 2. *The values of thickness (m), area (km^2), volume (km^3), cumulative volume (km^3) and the percentage of volume for each isopach.*

	Bulk Volume (km^3)	DRE Volume (km^3)
Preserved extra-caldera ignimbrite volume	56 – 67	22.0 – 26.4
Marine volume	56 – 67	22.0 – 26.4
Intracaldera volume	16 – 43.2	7.9 – 21.4
Areal erosion	9.6	3.7
Co-ignimbrite ash volume	273.4 – 364.7	107.6 – 143.5
Total PDC volume	411 – 561.1	163.2 – 225.1
Fallout volume (Marti et al., 2016; Perrotta & Scarpati, 2003)	4 – 54	1.7 – 22.6
Total CI volume	415 – 615.1	164.9 – 247.7

Table 3. *The volume of the CI eruption. The various parts of the PDC volume estimate are explained in the text. The fallout volume considered in this work is the maximum and the minimum proposed in literature by Perrotta and Scarpati (2003) and Marti et al. (2016).*

Figures

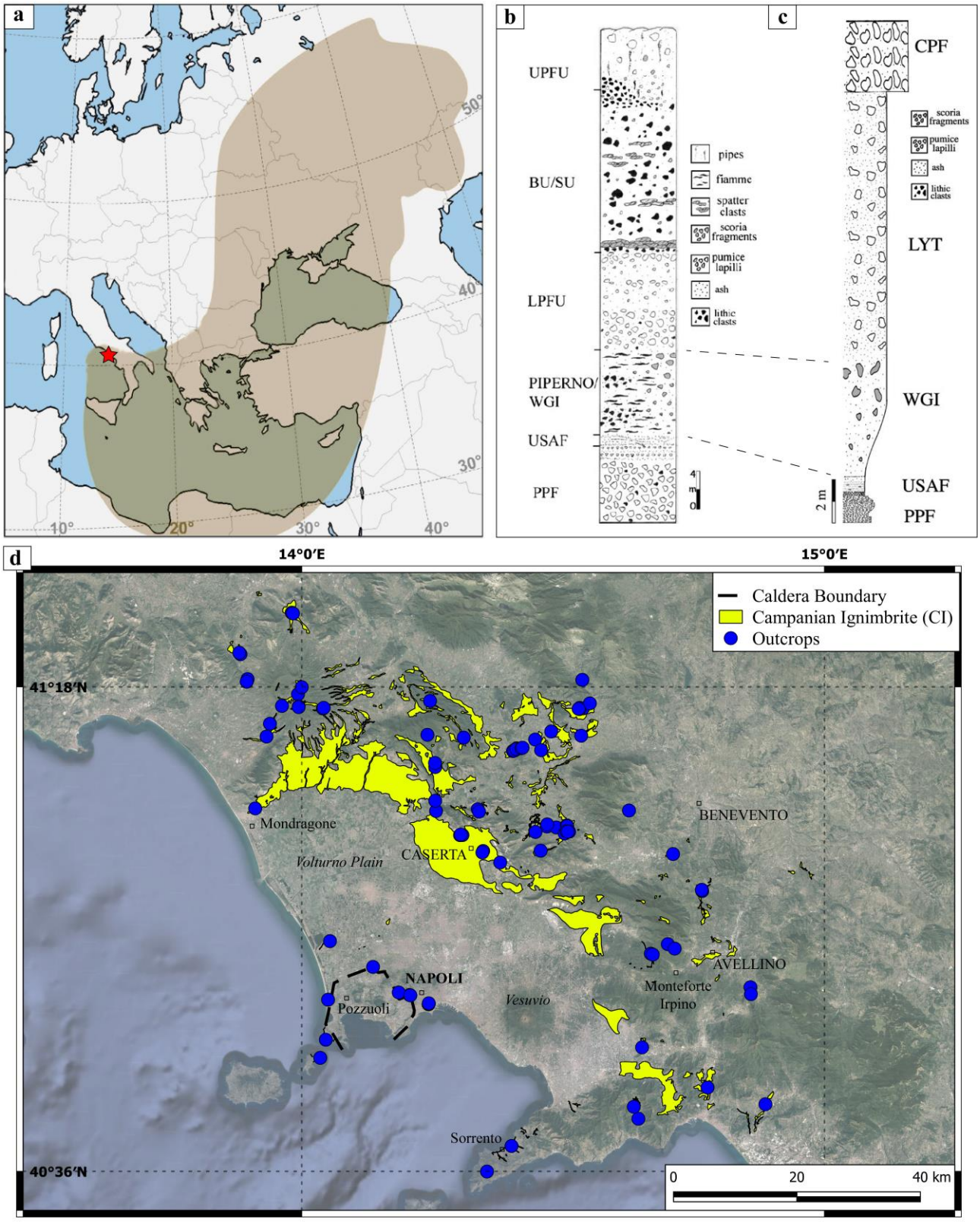

Figure 1. *The Campanian Ignimbrite distribution.* ***(a)*** *Dispersal area of the CI tephra from the Campi Flegrei caldera (red star), modified from Giaccio et al. (2017). Stratigraphic type-sections of CI proximal* ***(b)*** *and distal* ***(c)*** *deposits modified from Fedele et al. (2008) and Cappelletti et al. (2003), respectively.* ***(d)*** *The*

Campanian Ignimbrite distribution in the Campanian region (the base map is from Google Satellite). Blue dots indicate the location of the studied outcrops (coordinates are reported in Appendix). The maps were generated using the QGIS Open-Source 3.4 (https://www.qgis.org/it/site/).

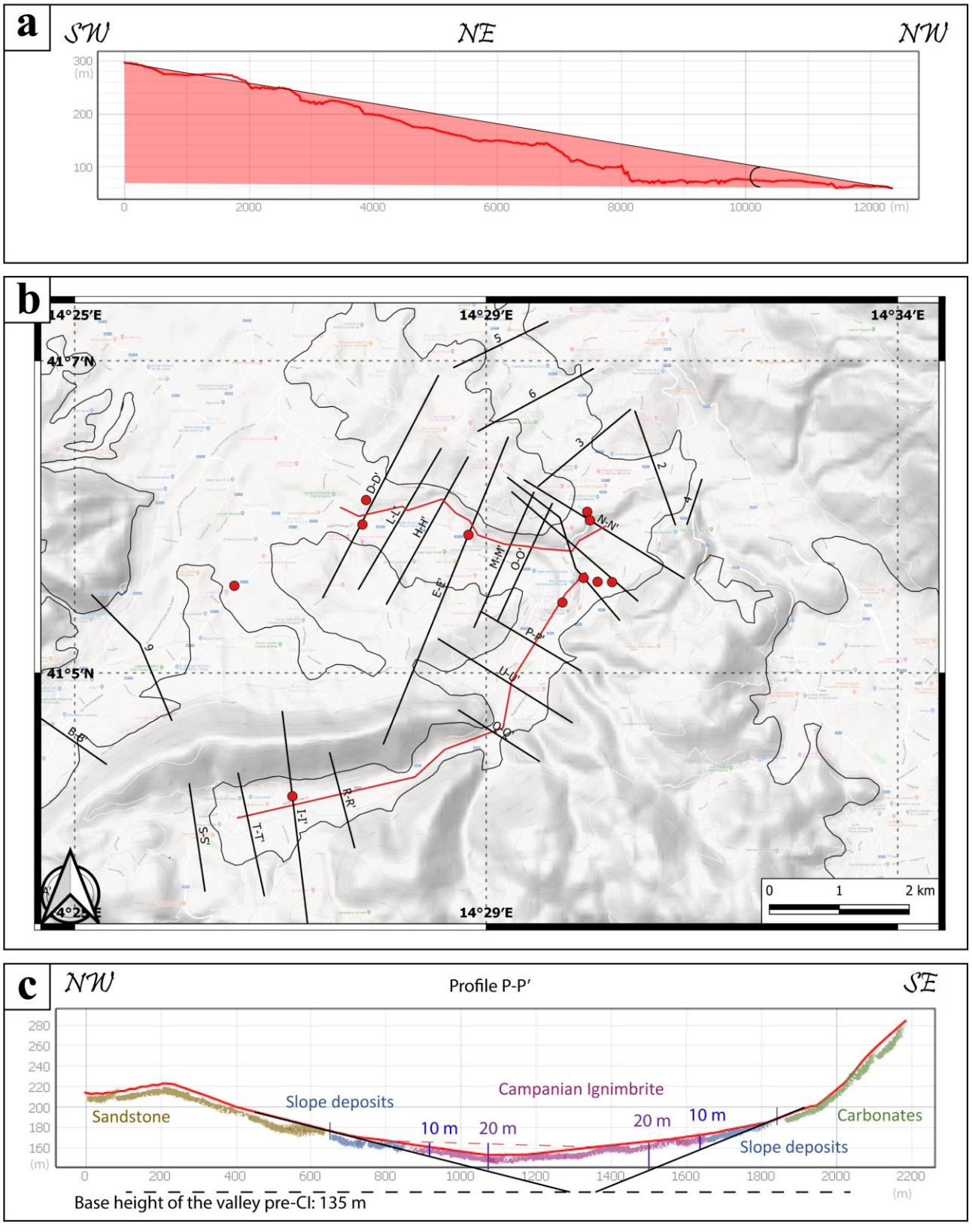

Figure 2. *The topography reconstruction in the Sant'Agata dei Goti area.* ***(a)*** *The modern valley is used as a reference for the paleo-slope during the CI eruption.* ***(b)*** *A series of profiles traced to study the paleo-valley; the red dots are outcrops where the CI is exposed.* ***(c)*** *Reconstruction of the paleo-valley in profile P-P', the base elevation is constrained to the CI base observed by fieldwork and to the current slope of the valley. The resulting thickness is always coherent with fieldwork, so where thicknesses are too high, they weren't considered and the isopachs were traced up to a realistic thickness. The numbers represent the thickness of the CI in meters.*

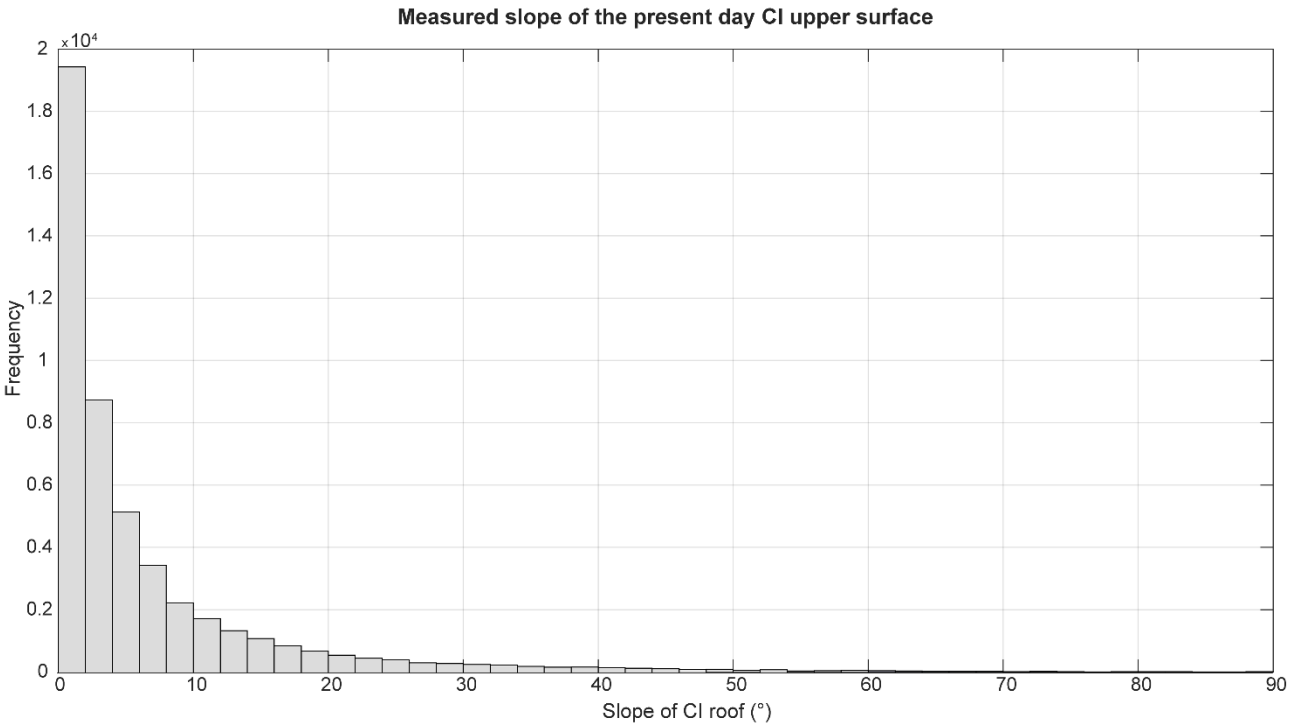

Figure 3. *Frequency of the slope of the upper surface of the CI. At least 80% of the exposed CI upper surface slopes less than 10°.*

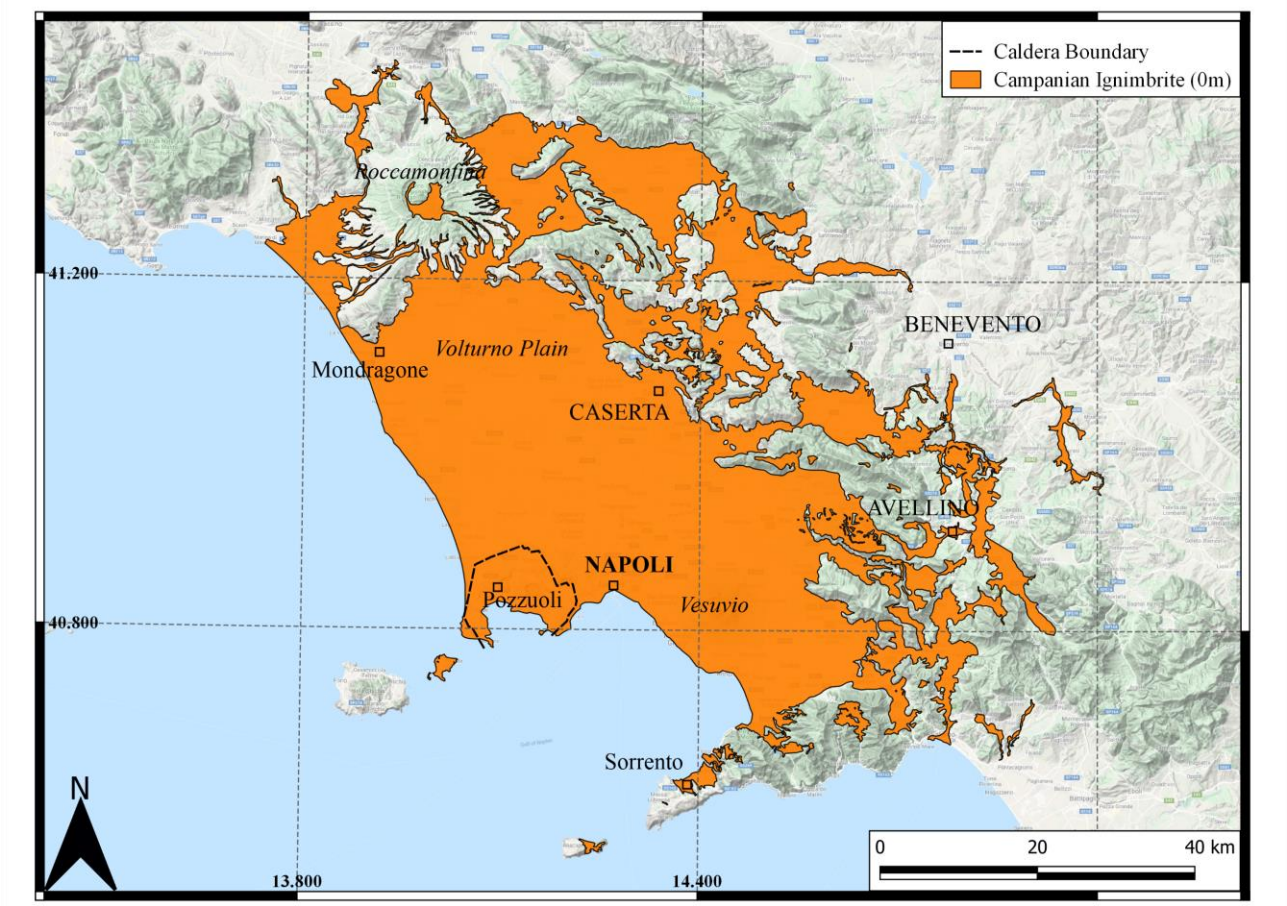

1056

1057 ***Figure 4.*** *The areal extent of the CI, enclosed within the isopach 0 m is shown in orange. The total area*
1058 *covered by the preserved deposits of CI is 3216 km^2, the envelopment with a shape is equal to 7547 km^2.*

1059

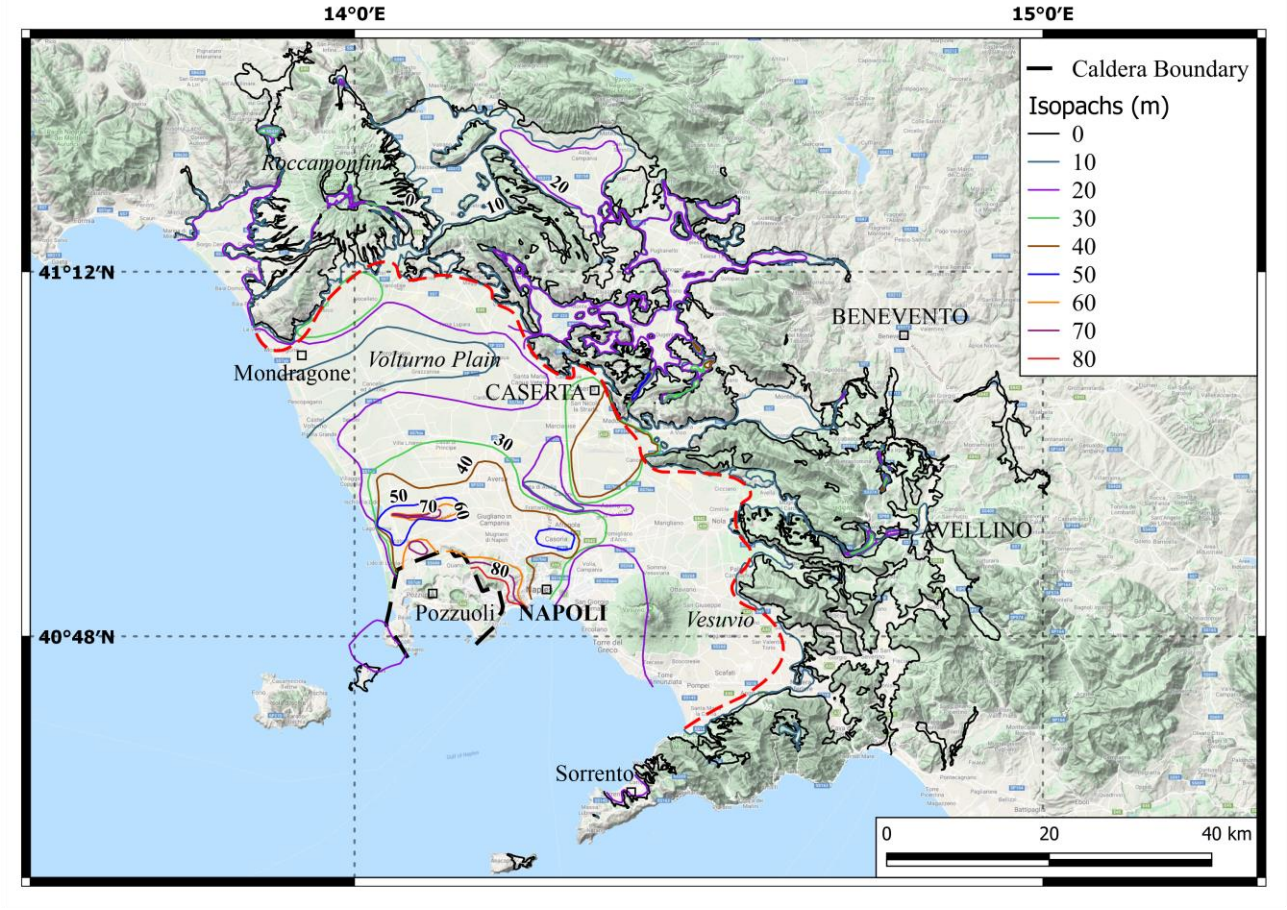

1060

1061 ***Figure 5.*** *Isopach map of the preserved extra-caldera deposits of the Campanian Ignimbrite. This map refers*
1062 *only to the pyroclastic density current deposits; it excludes the Plinian fallout and the co-ignimbrite ash. The*
1063 *different colors for each isopach are reported in the map key. The red dashed line divides the proximal and*
1064 *the distal area.*

1065

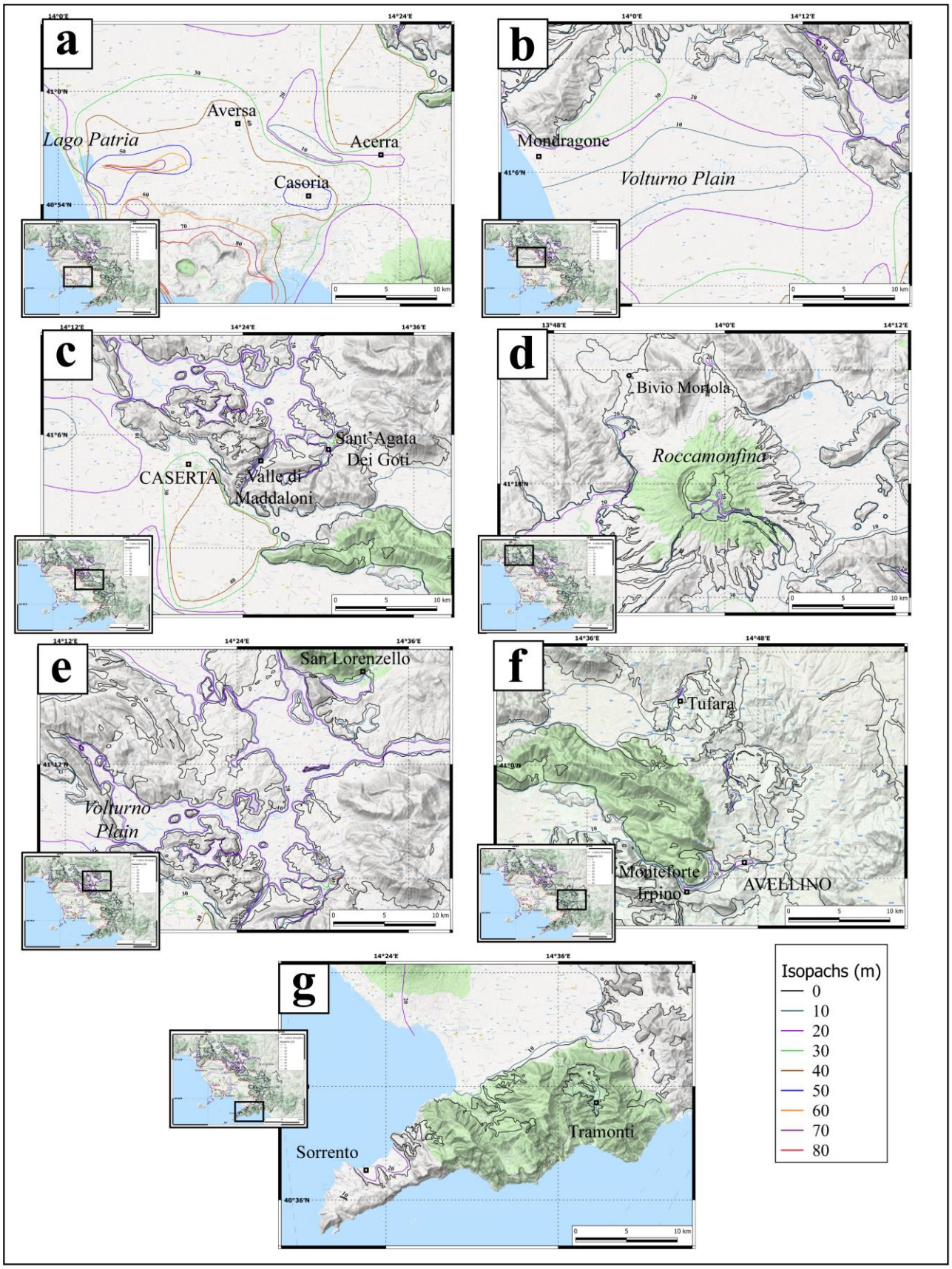

Figure 6. *Detailed isopach maps of selected areas of the Campanian Ignimbrite (excludes fallout):* ***(a)*** *north of the caldera, between Lago Patria and Acerra;* ***(b)*** *northern part of the Campanian Plain;* ***(c)*** *Apennine ridges east of the Campi Flegrei caldera and the Valley of Maddaloni;* ***(d)*** *Roccamonfina and Mortola, in the*

north of the studied area; ***(e)*** *Volturno plain and San Lorenzello area, northeast of the caldera;* ***(f)*** *distal area of Avellino, southeast of the caldera;* ***(g)*** *Sorrento peninsula, in the southern part of the studied area.*

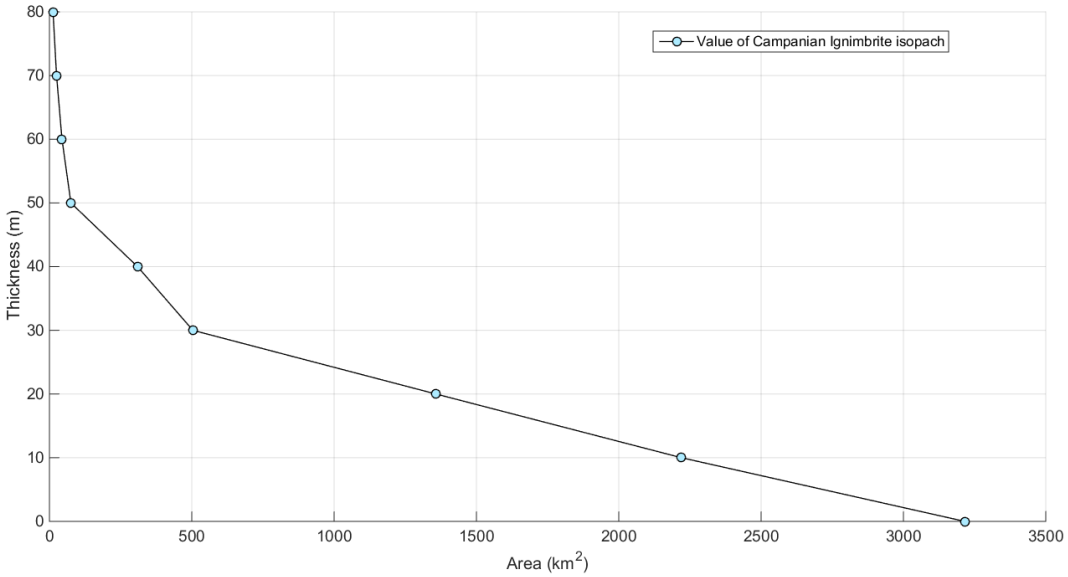

Figure 7. *The thickness (m) plotted against the area (km^2) of each isopach of the preserved deposits of the CI PDC. The volume is the subtended area of this plot.*

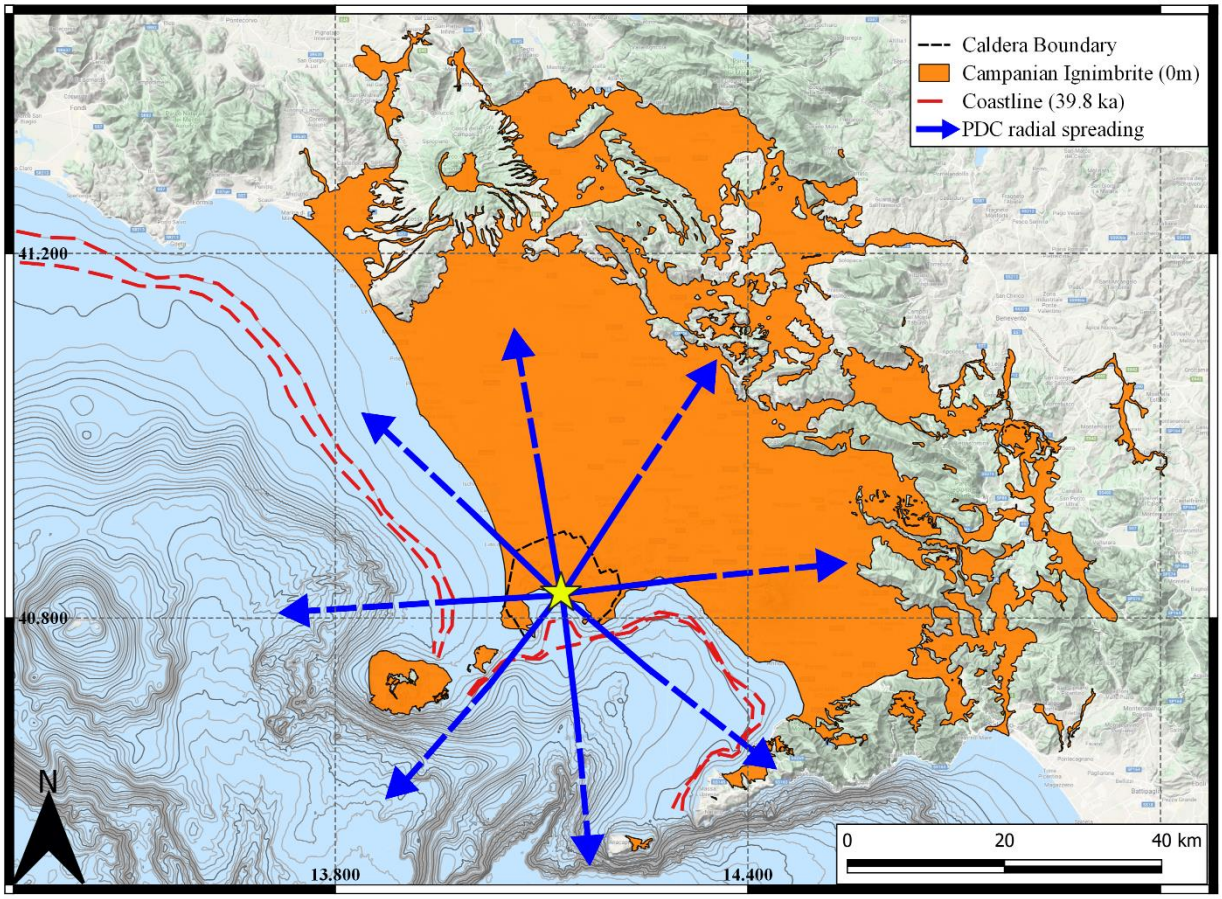

Figure 8. *Bathymetry of the submerged area of the Campi Flegrei Caldera. The red line is the 40 ka coastline, equivalent to -75 – -87 m of the present one. The blue arrows indicate the possible radial spreading of the PDC based on outcrops disposed radially from the center of the Caldera (yellow star) and turbidity currents in the Tyrrhenian Sea.*

Geochemistry, Geophysics, Geosystems

Supporting Information for

Detailed evaluation of PDC's volume for large eruptions: the case of the 39.8 ka Campanian Ignimbrite, Italy

Aurora Silleni[1#], Guido Giordano[1], Roberto Isaia[2], Michael H. Ort[3]

1- Dipartimento di Scienze, Università di Roma Tre, Largo S. Leonardo Murialdo 1, 00146, Rome, Italy

2- Istituto Nazionale di Geofisica e Vulcanologia, Osservatorio Vesuviano, Via Diocleziano 328, 80124 Naples, Italy

3- SES, Box 4099, Northern Arizona University, Flagstaff, AZ 86011-4099, USA

Contents of this file

Introduction

This supporting information explains how the errors and uncertainties related to the ignimbrite volume were calculated. These were estimated as 1.6 km^3 in proximal area and 3.9 km^3 in distal area.

Data related to the location of outcrops and density are reported in the Repository Data online at https://mfr.osf.io/render?url=https%3A%2F%2Fosf.io%2F3a6bz%2Fdownload.

S1 - The volume uncertainties.

The uncertainties were determined by two different methods, one for the proximal area and one for the distal. In the first case, the proximal isopach map was traced fitting thickness data. In order to avoid subjective interpretation, a second isopach map was delineated tracing isopachs differently, but always consistent with data. A new volume was calculated from this second convincing proximal isopach map. The percentage

difference with the first map was estimated (3.06%) corresponding to a volume of 1.6 km3.
The main error in estimating the paleo-valley topography is the extrapolation of the base elevation of the valley itself. For this reason, in the area of Altavilla Irpina, the profiles were modified, and the base elevations were adjusted to reach the maximum difference possible in altitude, always constrained by field data. The volume diverged by 25%, corresponding to a volume of 3.9 km3. The total CI volume uncertainties are 5.5 km3.

Supplementary data

Data from literature inserted into the GIS database are reported in Table A.1. Moreover, other papers were used for geological sketches, proximal area isopach maps and isopleths maps (Aprile et al., 2004; Arienzo et al., 2009, 2011; Bellucci, 1994; F. G. Fedele et al., 2002; L. Fedele et al., 2016; Fowler et al., 2007; Giaccio et al., 2008; Incoronato & Nardi, 1987; Milia & Torrente, 2007; Ortolani & Aprile, 1985; Pappalardo et al., 2008; Scandone et al., 1991; Scarpati & Perrotta, 2016; Signorelli et al., 1999; Smith et al., 2016; de Vivo et al., 2010). Outcrops location are reported in Table A.2.

ID	Paper	Latitude (°)	Longitude (°)	Thickness (m)	Name
1	Barberi et al. (1978)	41.05698	14.33346	14.9	S. Nicola La Strada
2	Barberi et al. (1978)	41.05573	14.70687	15.5	Tufara
3	Barberi et al. (1978)	40.94861	14.56534	41.0	Tufino
4	Cappelletti et al. (2003)	41.06165	14.42083	7.0	Balzarama
5	Cappelletti et al. (2003)	41.11082	14.47346	8.3	Dugenta
6	Cappelletti et al. (2003)	40.94280	14.60260	12.1	La schiava
7	Cappelletti et al. (2003)	41.23293	14.50691	4.3	Faicchio
8	Cappelletti et al. (2003)	40.77209	14.66155	20.9	Castel San Giorgio
9	Cappelletti et al. (2003)	40.95816	15.00003	7.1	San Mango S. C.
10	De Vivo et al. (2001)	40.94472	14.16421	19.6	Giugliano
11	De Vivo et al. (2001)	40,93534	14,56743	3.8	Taurano
12	De Vivo et al. (2001)	41.17565	14.49265	10.1	Sant'Agata dei Goti
13	De Vivo et al. (2001)	41.06337	14.70339	10.6	Altavilla
14	De Vivo et al. (2001)	40.97126	14.54410	10.7	Tufino
15	De Vivo et al. (2001)	40.95244	14.55400	10.1	Sperone
16	De Vivo et al. (2001)	40.87905	14.29606	8.9	Ponti Rossi
17	De Vivo et al. (2001)	40.88207	14.31975	5.1	Poggioreale
18	De Vivo et al. (2001)	40.79846	14.04573	9.0	Monte di Procida
19	De Vivo et al. (2001)	40.62828	14.37821	10.3	Sant'Agnello
20	De Vivo et al. (2001)	40.87633	14.34249	6.8	Arpino

21	De Vivo et al. (2001)	40.54981	14.23133	10.4	Capri
22	L. Fedele et al. (2008)	40.76367	14.03370	9.8	Punta della lingua
23	L. Fedele et al. (2008)	40.76784	14.01611	27.0	Scotto di Carlo
24	L. Fedele et al. (2008)	40.79131	14.05739	25.7	Monte di Procida
25	L. Fedele et al. (2008)	40.84665	14.05135	10.2	Cuma
26	L. Fedele et al. (2008)	40.89064	14.07671	6.0	San Severino
27	L. Fedele et al. (2008)	40.88900	14.10608	17.0	Spinelli
28	L. Fedele et al. (2008)	40.90952	14.09640	14.0	Zaccaria
29	L. Fedele et al. (2008)	40.92155	14.11957	24.0	Qualiano
30	L. Fedele et al. (2008)	40.90092	14.14108	18.9	Punta Marmolite
31	L. Fedele et al. (2008)	40.88169	14.16774	5.1	Quarto
32	L. Fedele et al. (2008)	40.85687	14.18742	72.0	Camaldoli
33	L. Fedele et al. (2008)	40.84269	14.22948	7.4	San Martino Hill
34	L. Fedele et al. (2008)	40.85087	14.23347	9.1	Montesanto
35	L. Fedele et al. (2008)	40.86016	14.22790	6.1	Fontanelle
36	L. Fedele et al. (2008)	40.87866	14.25874	4.5	Ponti Rossi
37	L. Fedele et al. (2008)	40.88394	14.27807	14.0	Santa Maria del pianto
38	Giaccio et al. (2006)	40.86797	14.85653	13.1	Serino
39	Langella et al. (2013)	40.88284	14.66613	3.6	Moschiano
40	Langella et al. (2013)	41.06646	14.71668	3.7	Tufara
41	Langella et al. (2013)	40.70136	14.62501	8.8	Pucara
42	Langella et al. (2013)	40.69312	14.83241	8.2	Torrente Sordina
43	Langella et al. (2013)	41.36129	13.86913	7.2	Mortola
44	Langella et al. (2013)	40.60310	14.35675	2.4	Monticchio
45	Langella et al. (2013)	41.12660	14.45214	8.2	Dugenta
46	Langella et al. (2013)	41.07085	14.39716	6.5	Balzarama
47	Langella et al. (2013)	41.04894	14.38355	11.6	Maddaloni
48	Langella et al. (2013)	41.01588	14.75955	12.1	Altavilla

49	Langella et al. (2013)	40.95232	14.58959	12.0	La schiava
50	Langella et al. (2013)	41.09617	14.45043	3.9	S. Agata dei Goti
51	Melluso et al. (1995)	40.84929	14.04881	15.6	Cuma
52	Melluso et al. (1995)	40.79063	14.04569	20.1	Marina di Vitafumo
53	Melluso et al. (1995)	40.76432	14.03661	13.5	Punta della lingua
54	Melluso et al. (1995)	40.76609	14.02101	23.6	Scotto di Carlo
55	Melluso et al. (1995)	40.76252	14.00877	10.1	Cimitero
56	Milia et al. (2003)	40.77427	14.43946	25.2	Trecase
57	Orsi and Rosi (1991)	40.89444	14.13328	16.0	Punta Marmolite
58	Orsi and Rosi (1991)	40.84473	14.04803	13.7	Cuma
59	Orsi and Rosi (1991)	40.79548	14.04394	9.7	Monte di Procida
60	Orsi and Rosi (1991)	40.71367	13.95586	1.3	Ischia grotte di terra
61	Orsi and Rosi (1991)	40.74482	13.99483	5.3	Vivara
62	Orsi and Rosi (1991)	40.76353	14.01032	10.2	Procida Pozzo vecchio
63	Orsi and Rosi (1991)	40.76622	14.02152	19.8	Procida scoglio cannone
64	Orsi and Rosi (1991)	40.76470	14.03672	17.2	Procida Punta della lingua
65	Orsi and Rosi (1991)	40.78996	14.04678	28.5	Marina di Vitafumo
66	Orsi and Rosi (1991)	40.80904	14.04393	19.5	Torregaveta
67	Orsi and Rosi (1991)	40.87962	14.07540	5.6	San Severino
68	Orsi and Rosi (1991)	40.85386	14.19331	79.2	Camaldoli
69	Orsi and Rosi (1991)	40.95268	14.11209	30.4	Scarafea
70	Orsi and Rosi (1991)	40.87458	14.26099	8.0	Ponti Rossi
71	Orsi and Rosi (1991)	40.65581	14.43023	7.6	Vico Equense
72	Orsi and Rosi (1991)	40.92946	14.70306	0.7	Acqua Fidia
73	Orsi and Rosi (1991)	41.26809	14.03841	1.6	Furnolo
74	Orsi and Rosi (1991)	41.12338	13.90684	2.6	Mondragone
75	Orsi and Rosi (1991)	40.71908	14.78138	0.3	Pellezzano
76	Orsi and Rosi (1991)	41.29998	13.99325	0.9	Roccamonfina

77	Orsi and Rosi (1991)	41.22075	14.12802	0.8	Visciano
78	Orsi and Rosi (1991)	41.27260	14.52178	8.6	Massa
79	Orsi et al. (1996)	40.85020	14.20771	80.0	Verdolino Valley
80	Orsi et al. (1996)	40.84979	14.19188	80.0	Torre di Franco
81	Orsi et al. (1996)	40.87559	14.31236	26.0	66
82	Orsi et al. (1996)	40.87037	14.30095	15.3	67
83	Orsi et al. (1996)	40.87446	14.29572	48.1	4
84	Orsi et al. (1996)	40.87704	14.29033	8.9	61
85	Orsi et al. (1996)	40.88727	14.29953	12.4	65
86	Orsi et al. (1996)	40.87741	14.26781	30.0	51
87	Orsi et al. (1996)	40.87480	14.24930	33.0	46
88	Orsi et al. (1996)	40.87765	14.22415	33.1	36
89	Orsi et al. (1996)	40.90006	14.22256	28.9	34
90	Orsi et al. (1996)	40.90738	14.24090	8.6	44
91	Orsi et al. (1996)	40.90336	14.26784	57.2	49
92	Orsi et al. (1996)	40.84838	14.05607	15.0	Cuma
93	Orsi et al. (1996)	40.86702	14.26767	6.0	Ponti Rossi
94	Orsi et al. (1996)	40.87882	14.08267	17.0	San Severino
95	Orsi et al. (1996)	40.86954	14.30927	4.0	Sant'Arpino
96	Orsi et al. (1996)	40.88741	14.15640	18.2	Trefola
97	Ort et al. (2003)	41.01429	14.76629	34.8	Altavilla
98	Ort et al. (2003)	41.27794	14.53083	12.5	Massa
99	Ort et al. (2003)	41.13269	13.89663	6.1	Mondragone
100	Pappalardo et al. (2002)	40.87216	14.26782	30.1	Ponti Rossi
101	Perrotta et al. (2006)	40.83247	14.24658	0.0	8
102	Perrotta et al. (2006)	40.83744	14.22889	0.0	1
103	Perrotta et al. (2006)	40.83885	14.23355	0.0	2
104	Perrotta et al. (2006)	40.84008	14.23731	0.0	3

105	Perrotta et al. (2006)	40.84207	14.24123	14.4	4
106	Perrotta et al. (2006)	40.84634	14.24016	15.5	5
107	Perrotta et al. (2006)	40.86076	14.23170	6.2	6
108	Perrotta et al. (2006)	40.85981	14.23585	2.0	I
109	Perrotta et al. (2006)	40.83756	14.24999	10.0	II
110	Perrotta et al. (2006)	40.83270	14.24157	21.7	III
111	Perrotta et al. (2010)	40.81133	14.07042	0.0	10
112	Perrotta et al. (2010)	40.80816	14.04338	5.6	11
113	Perrotta et al. (2010)	40.79909	14.03731	5.6	12
114	Perrotta et al. (2010)	40.79504	14.04368	5.6	13
115	Perrotta et al. (2010)	40.78831	14.05603	2.9	14
116	Perrotta et al. (2010)	40.78932	14.06303	0.9	15
117	Perrotta et al. (2010)	40.75982	14.02430	7.4	1
118	Perrotta et al. (2010)	40.75991	14.03198	0.0	2
119	Perrotta et al. (2010)	40.76759	14.01905	26.3	3
120	Perrotta et al. (2010)	40.76807	14.00989	0.0	4
121	Perrotta et al. (2010)	40.76457	14.01012	9.2	5
122	Perrotta et al. (2010)	40.76275	14.00877	9.8	6
123	Perrotta et al. (2010)	40.76039	14.00850	3.0	7
124	Perrotta et al. (2010)	40.75873	14.00936	5.2	8
125	Perrotta et al. (2010)	40.74480	13.99123	2.1	9
126	Rolandi et al. (2003)	41.05877	14.42550	3.1	Maddaloni
127	Rolandi et al. (2003)	41.06104	14.46361	14.7	Durazzano
128	Rolandi et al. (2003)	40.89955	14.65636	4.9	Taurano
129	Rolandi et al. (2003)	40.88146	14.68907	11.1	Moschiano
130	Rolandi et al. (2003)	40.81916	14.67199	18.8	Sarno
131	Rolandi et al. (2003)	40.80551	14.70470	7.7	Siano
132	Rolandi et al. (2003)	40.78712	14.70638	34.4	Castel San Giorgio

133	Rolandi et al. (2003)	40.66237	14.44305	15.5	Seiano Valley
134	Rolandi et al. (2003)	40.62574	14.41407	9.9	Piano di Sorrento
135	Rolandi et al. (2003)	40.76290	14.03357	20.5	Punta della lingua
136	Rolandi et al. (2003)	40.79092	14.04556	22.0	Marina di Vitafumo
137	Rolandi et al. (2003)	40.81290	14.04381	27.5	Torregaveta
138	Rolandi et al. (2003)	40.78915	14.06432	3.0	Miliscola
139	Rolandi et al. (2003)	40.84768	14.05100	15.4	Cuma
140	Rolandi et al. (2003)	40.89771	14.14052	13.8	Punta Marmolite
141	Rolandi et al. (2003)	40.85252	14.19673	58.2	Camaldoli
142	Rolandi et al. (2003)	40.84307	14.21673	162.0	Vomero
143	Rolandi et al. (2003)	40.84287	14.24107	17.8	San Martino
144	Rolandi et al. (2003)	40.86743	14.27793	27.1	Ponti Rossi
145	Rolandi et al. (2003)	40.87120	14.29386	26.3	Poggioreale
146	Rolandi et al. (2003)	40.87720	14.31490	5.2	Arpino
147	Rolandi et al. (2003)	40.83655	14.25039	43.0	Palazzo Reale
148	Rolandi et al. (2003)	40.78112	14.44386	50.0	Trecase
149	Rosi et al. (1988)	40.71199	13.96250	0.7	Grotta di Terra
150	Rosi et al. (1988)	40.79707	14.04236	12.6	Monte di Procida - 6
151	Rosi et al. (1988)	40.78973	14.05386	5.3	Monte di Procida - 5
152	Rosi et al. (1988)	40.74315	13.99227	1.6	Vivara - 2
153	Rosi et al. (1988)	40.76072	14.00861	5.0	Procida - 3
154	Rosi et al. (1988)	40.76522	14.01056	11.7	Procida - 4
155	Rosi et al. (1996)	40.71287	13.95659	1.3	Ischia grotte di terra
156	Rosi et al. (1996)	40.74326	13.99649	5.5	Vivara
157	Rosi et al. (1996)	40.76308	14.01249	11.0	Pozzo vecchio
158	Rosi et al. (1996)	40.76653	14.02035	20.4	Scoglio cannone
159	Rosi et al. (1996)	40.76444	14.03693	16.8	Punta della lingua
160	Rosi et al. (1996)	40.78999	14.04661	26.6	Vitafumo

161	Rosi et al. (1996)	40.81117	14.04389	21.0	Torregaveta
162	Rosi et al. (1996)	40.84822	14.04739	15.1	Cuma
163	Rosi et al. (1996)	40.88104	14.07809	5.2	San Severino
164	Rosi et al. (1996)	40.89488	14.13404	21.5	Punta Marmolite
165	Rosi et al. (1996)	40.85590	14.19588	77.2	Camaldoli
166	Rosi et al. (1996)	40.95234	14.11780	26.3	Scarafea
167	Rosi et al. (1996)	40.87618	14.26290	7.4	Ponti Rossi
168	Giaccio (2006)	40.86320	14.86388	12.4	Serino
169	Rosi and Sbrana (1987)	40.85786	14.19574	25.0	Camaldoli
170	Rosi and Sbrana (1987)	40.90527	14.14250	13.0	Punta Marmolite
171	Rosi and Sbrana (1987)	40.88230	14.06558	1.1	San Severino
172	Sparice (2015)	41.40636	13.98329	10.3	Mignano Monte Lungo
173	Sparice (2015)	41.28622	13.99279	4.3	Roccamonfina
174	Sparice (2015)	41.26915	14.03347	10.0	Furnolo
175	Sparice (2015)	41.18818	13.97548	10.0	Carinola
176	Sparice (2015)	41.12329	13.90834	4.9	Mondragone
177	Sparice (2015)	41.13758	14.25327	7.1	Triflisco
178	Sparice (2015)	41.16939	14.26525	8.0	Casella1
179	Sparice (2015)	41.19606	14.23739	3.0	Casella2
180	Sparice (2015)	41.20890	14.40448	5.0	Ruviano
181	Sparice (2015)	41.27236	14.46645	8.2	Faicchio
182	Sparice (2015)	41.27024	14.51387	3.2	S. Lorenzello I
183	Sparice (2015)	41.26833	14.53105	8.2	San Lorenzello II
184	Sparice (2015)	41.12278	14.43879	8.2	Dugenta
185	Sparice (2015)	41.09454	14.48905	20.5	S. Agata dei Goti
186	Sparice (2015)	41.08609	14.54280	4.5	Moiano
187	Sparice (2015)	41.12554	14.62174	21.0	Tocco Claudio
188	Sparice (2015)	41.02847	14.69167	4.6	Roccabascerana

189	Sparice (2015)	41.05333	14.71525	3.6	Tufara
190	Sparice (2015)	41.06472	14.88412	1.0	Poeti
191	Sparice (2015)	41.00583	14.76202	20.4	Altavilla Irpina
192	Sparice (2015)	41.06822	15.04053	3.0	Grottaminarda
193	Sparice (2015)	40.97184	14.96672	8.5	S. Mango sul calore
194	Sparice (2015)	40.93227	14.70449	1.1	Acqua Fidia
195	Sparice (2015)	40.91711	14.67449	6.6	Monteforte Irpino 1
196	Sparice (2015)	40.89668	14.66921	6.6	Monteforte Irpino 2
197	Sparice (2015)	40.87410	14.67623	1.7	Monteforte irpino 3
198	Sparice (2015)	40.89039	14.63113	5.0	Visciano 1
199	Sparice (2015)	40.90129	14.62203	5.0	Visciano2
200	Sparice (2015)	40.86459	14.70745	4.7	Moschiano
201	Sparice (2015)	40.87153	14.82712	0.7	Aiello sul sabato
202	Sparice (2015)	40.83936	14.89030	4.3	Serino
203	Sparice (2015)	40.82302	14.91053	7.0	Sala
204	Sparice (2015)	40.81967	14.81731	0.5	Montoro superiore
205	Sparice (2015)	40.75354	14.80000	1.5	Penta
206	Sparice (2015)	40.77694	14.65092	1.9	S.Anna
207	Sparice (2015)	40.73088	14.70338	0.5	S.Lucia
208	Sparice (2015)	40.71625	14.77207	5.1	Cologna
209	Sparice (2015)	40.69339	14.88640	6.9	Fosso di Prepezzano
210	Sparice (2015)	40.67902	14.85191	16.1	Sordina
211	Sparice (2015)	40.69618	14.63176	4.6	Polvica
212	Sparice (2015)	40.67848	14.63972	10.7	Paterno S. Arcangelo
213	Sparice (2015)	40.63868	14.40205	20.7	Piano di Sorrento
214	Sparice (2015)	40.61669	14.38275	1.6	Cesarano
215	Sparice (2015)	40.59932	14.35159	3.4	Monticchio
216	Aprile and Toccaceli (2002)	40.81330	14.61202	24.3	Pozzo SSLM6

217	Aiello et al. (2018)	41.112175	13.904175	16.9	LV4
218	Costanzo and Nunziata (2019)	40.83715	14.25036	10.0	S97
219	Costanzo and Nunziata (2019)	40.84192	14.24980	4.9	S95
220	Nunziata et al. (2004)	40.86762	14.30477	16.1	Site 2 - S67
221	Nunziata et al. (2004)	40.87512	14.27622	8.0	Site 3
222	Torrente et al. (2010)	40.93713	14.11618	75.6	16
223	Torrente et al. (2010)	40.82895	14.22241	18.7	67
224	Torrente et al. (2010)	40.82960	14.24913	83.5	75
225	Torrente et al. (2010)	40.83690	14.25605	42.9	78
226	Torrente et al. (2010)	40.84064	14.24542	13.6	81b
227	Torrente et al. (2010)	40.84729	14.24480	13.9	81c
228	Torrente et al. (2010)	40.85683	14.27695	29.7	100
229	Torrente et al. (2010)	40.86468	14.29650	24.7	103
230	Torrente et al. (2010)	40.87460	14.29625	39.8	110
231	Torrente et al. (2010)	40.88993	14.28339	39.2	114
232	Torrente et al. (2010)	40.90919	14.31455	60.8	118
233	Torrente et al. (2010)	40.89068	14.33805	16.1	141
234	Torrente et al. (2010)	40.87740	14.21536	107.4	590
235	Torrente et al. (2010)	40.84317	14.22551	79.6	665
236	Torrente et al. (2010)	40.85645	14.23688	64.0	667
237	Torrente et al. (2010)	40.89704	14.29650	50.3	1021
238	Torrente et al. (2010)	40.98579	14.17752	37.0	T163

Table A.1. *Outcrops used in the GIS database, the relative coordinates were taken from the papers or from the georeferenced map, produced during this work.*

ID	Site name	Latitude (°)	Longitude (°)	Altitude (m) a.s.l.	Units	Observed Thickness (m)
1	Stop 1 - Mignano Montelungo	41.40661	13.98082	95	WGI	8
2	Stop 2 - Mignano Montelungo	41.40628	13.98121	100	USAF, WGI	1
3	Stop 3 - Mignano Montelungo	41.40629	13.98113	110	USAF, WGI	1
4	Stop 4 - Roccamonfina	41.28944	13.99278	540	GL, USAF, WGI	50
5	Stop 5 - Roccamonfina	41.28952	13.99265	560	WGI	4
6	Stop 6 - Sessa Aurunca	41.24711	13.93903	185	WGI	12
7	Ponte Sant'Agata	41.22863	13.93258	139	WGI	30
8	SP14	41.27269	13.9621	545	WGI	25
9	Stop 7 - Tavola	41.29957	14.00002	610	USAF, WGI	2
10	Stop 8 - Torano A	41.27172	13.99416	440	WGI	1
11	Stop 8 - Torano B	41.269	14.04052	461	GL, USAF, WGI	30
12	Stop 9 - Furnolo	41.27165	13.99404	301	GL, USAF, WGI	2
13	Stop 10 - Furnolo	41.26993	14.0419	300	WGI	35
14	Comune Mignano Montelungo	41.40541	13.98322	130	WGI	6
15	Stop 11 - Sant'Angelo in Formis	41.12139	14.25682	57	USAF, WGI	15
16	Stop 12 - Triflisco	41.1362	14.25528	34	WGI	5
17	Stop 13 - Pontelatone A	41.18584	14.25546	83	WGI	1
18	Stop 13 - Pontelatone B	41.1854	14.25557	81	WGI	5
19	Stop 14 - Pontelatone	41.18474	14.2553	78	USAF, WGI	5
20	Stop 15 - Pontelatone SP189	41.1906	14.25493	98	WGI	7
21	Stop 16 - Ruviano	41.20994	14.4079	78	WGI	2
22	Stop 17 - Ruviano	41.20936	14.40745	70	WGI	21
23	Stop 18 - San Salvatore Telesino	41.23581	14.47714	104	WGI	2
24	Stop 19 - Puglianello	41.22433	14.4464	62	WGI	3
25	Telese terme	41.22982	14.53457	116	WGI	2
26	Ruviano 1	41.21043	14.41082	57	WGI	5
27	Ruviano Fosso	41.21167	14.41127	63	WGI	8
28	Ruviano 2	41.21055	14.41012	64	WGI	3
29	Stop 20 - San Lorenzello	41.26985	14.53162	190	USAF, WGI	19
30	Stop 21 - San Lorenzello	41.2692	14.53801	214	WGI	9
31	Stop 22 - Amorosi	41.20903	14.45779	60	WGI	2
32	Stop 23 - Casagiove	41.08671	14.30732	67	WGI	7
33	San Lorenzello	41.26818	14.53105	196	WGI	15
34	San Lorenzello - Cerreto	41.27637	14.55113	232	WGI	5
35	San Lorenzello Ristorante	41.2685	14.52962	191	WGI	10
36	Stop 24 - Casagiove	41.08662	14.30278	65	WGI	14
37	Stop 25 - Gradillo	41.12394	14.33669	166	WGI	24
38	Casagiove SS700	41.08747	14.30406	74	WGI	6

39	Gradillo	41.12054	14.33908	193	WGI	2
40	Ruviano 3	41.20775	14.40391	75	WGI	3
41	Ruviano 4	41.20849	14.40651	70	WGI	13
42	Ruviano 5	41.21053	14.41048	57	WGI	11
43	Ruviano - Cimitero	41.21192	14.42011	60	WGI	1
44	Ruviano 6	41.21258	14.42225	60	WGI	3
45	Stop 26 - Maddaloni	41.04716	14.37956	62	LYT	1
46	Cava abbandonata	41.06373	14.34691	56	LYT	5
47	Stop 27 - Caserta	41.06161	14.3455	53	LYT	4
48	Stop 28 - Sant'Anna	41.09116	14.44714	62	LYT	15
49	SP121	41.09902	14.46894	84	LYT	20
50	Stop 29 - Capellino	41.09769	14.48696	112	LYT	53
51	Ponte Sant'Agata dei Goti	41.08902	14.50297	148	WGI	40
52	Stop 30 - Durazzano	41.06417	14.45702	264	WGI	3
53	Sant'Agata dei Goti top	41.10065	14.50719	142	WGI	0
54	Stop 31 - San Pietro	41.09956	14.50764	126	WGI	43
55	Stop 32 - Castrone	41.09163	14.51141	147	LYT	3
56	Stop 33 - Sant'Agata dei Goti	41.09217	14.50656	107	USAF, GL, WGI	35
57	Stop 34 - Sant'Agata dei Goti	41.09167	14.50894	123	WGI, LYT	35
58	SP121 bis	41.10215	14.46956	84	LYT	2
59	Stop 35 - Tocco Caudio	41.12213	14.62599	485	LYT	1
60	Stop 36 - Tufara	41.05936	14.71026	198	PPF, WGI	20
61	Stop 37 - Altavilla Irpina B	41.00774	14.76531	260	LYT	20
62	Stop 37 - Altavilla Irpina A	41.00714	14.76552	244	PPF, GL, USAF, WGI, LYT	5
63	Lungofiume - Altavilla Irpina	41.00604	14.76601	222	WGI, LYT	14
64	Stop 38 - Monteforte Irpino	40.91418	14.67142	444	LYT	14
65	Stop 39 - Verdolino	40.85522	14.20769	153	PP, BM	50
66	Stop 40 - Monte di Procida	40.791	14.04602	0	PP, BM	3
67	Stop 41 - Mondragone	41.12515	13.91096	30	WGI	80
68	SS430 A	41.31125	13.89634	19	WGI	12
69	SS430 B	41.30749	13.89466	18	WGI	12
70	Stop 42 - Mortola	41.34702	13.88266	23	WGI	10
71	Stop 43 - Mortola 2	41.34902	13.88048	31	WGI	3
72	Stop 44 - Punta Marmolite	40.89635	14.13634	64	BM	7
73	Stop 45 - Acqua Fidia	40.92923	14.70025	958	PPF, GL, USAF, WGI	3
74	Piano Acqua Fidia	40.92281	14.7134	804	WGI	2
75	Cerreto Sannita	41.31006	14.53653	246	WGI	1
76	Stop 46 - Civitella	41.31012	14.5368	258	WGI	1
77	Stop 47 - Procida	40.76473	14.03531	0	BM	7
78	Stop 39 - Verdolino B	40.85571	14.20621	145	PP, LPFU	80
79	Stop 48 - Pianura	40.85935	14.18551	195	PP	10

80	Stop 49 - Vigna S. Martino 1	40.84231	14.24247	76	PPF, USAF, BM	8
81	Stop 50 - Vigna S. Martino 2	40.84301	14.24311	175	BM, UPFU	3
82	Stop 51 - Vigna S. Martino 3	40.84373	14.24292	152	PP	3
83	Stop 52 - Baiano	40.91548	14.66762	400	PPF	
84	Stop 53 - Cuma	40.84895	14.05028	55	BM, LPFU	20
85	Stop 54 - Lago Patria	40.93363	14.05399	37	WGI, BM	5
86	Stop 55 - Le Campole	41.23112	14.24032	583	WGI	1
87	Stop 56 - Liberi	41.22711	14.30978	421	WGI	1
88	Stop 57 - Statigliano	41.27991	14.24541	275	WGI	1
89	Stop 58 - Sant'Anna	40.77986	14.65101	124	WGI	10
90	Stop 59 - Paterno Sant'Arcangelo	40.67639	14.64385	167	WGI	5
91	Stop 60 - Polvica	40.69385	14.63513	278	WGI	4
92	Stop 61 - Monticchio	40.59983	14.35433	312	PPF, WGI	18
93	Stop 62 - Piano di Sorrento	40.6369	14.40127	18	WGI, LYT	25
94	Stop 63 - Fosso di Prepezzano	40.69748	14.88704	128	WGI	3
95	Stop 64 - Cologna	40.72163	14.7763	154	WGI	1
96	Stop 65 - Serino Cimitero	40.86696	14.85831	365	PPF, WGI	1
97	Stop 66 - Serino Ferrovia	40.85697	14.85926	390	WGI	2

Table A.2. *Data on outcrop locations: ID, site name, latitude, longitude, elevation, units and observed thickness for each outcrop.*

Density data used for the DRE volume, are reported in Table A.3.

Sample	Unit	ρ bulk (g/cm^3)	Standard deviation (g/cm^3)	Total porosity (%)
AS01	WGI	1.003	0.009	62
AS07	WGI	0.942	0.004	64
AS09	WGI	0.938	0.005	64
AS10	WGI	1.000	0.007	62
AS13	WGI	0.764	0.051	71
AS14	WGI	0.918	0.014	65
AS16	WGI	1.194	0.004	55
AS21	WGI	0.842	0.007	68
AS24	USAF-WGI	0.835	0.004	68
AS25	WGI	0.830	0.003	68
AS26	WGI	0.984	0.003	62
AS30	USAF-WGI	0.799	0.005	69
AS31	WGI	0.888	0.002	66
AS32	WGI	1.000	0.011	62
AS38	LYT	0.830	0.014	68
AS49	WGI	1.064	0.005	59
AS50	WGI	1.088	0.002	58
AS52	LYT	1.151	0.019	56
AS53	WGI	0.925	0.013	65
AS54	WGI	0.987	0.003	62
AS61	LYT	1.060	0.010	60
AS63	PIPERNO	1.283	0.001	49
AS69	PIPERNO	1.275	0.008	51
AS70	PIPERNO	1.302	0.002	49
AS73	WGI	0.816	0.003	69
AS75	WGI	0.959	0.005	63
ES03	WGI	1.008	0.014	62
ES04	WGI	0.843	0.057	68
ES05	WGI	1.050	0.010	60
ES08	WGI	1.155	0.011	56
ES10	WGI	1.330	0.003	49
ES11	LYT	0.885	0.021	66
ES12	WGI	1.047	0.003	60
ES14	WGI	1.063	0.004	60
ES17	WGI	0.999	0.014	62
ES18	WGI	1.080	0.012	59
ES19	WGI	1.002	0.023	62
ES20	WGI	0.745	0.015	72
ES21	WGI	1.074	0.019	59
ES22	WGI	1.153	0.006	56

Table A.3. *Values of bulk density (g/cm^3), and total porosity (the sum of open and closed porosity) for the analyzed samples. The standard deviation of density is given by the instrument. Samples were taken from all the Campanian Ignimbrite areal distribution and from different units.*

The volume uncertainties

The uncertainties were determined by two different methods, one for the proximal area and one for the distal. In the first case, the proximal isopach map was traced fitting thickness data. In order to avoid subjective interpretation, a second isopach map was delineated tracing isopachs differently, but always consistent with data. A new volume was calculated from this second convincing proximal isopach map. The percentage difference with the first map was estimated (3.06%) corresponding to a volume of 1.6 km^3.

The main error in estimating the paleo-valley topography is the extrapolation of the base elevation of the valley itself. For this reason, in the area of Altavilla Irpina, the profiles were modified, and the base elevations were adjusted to reach the maximum difference possible in altitude, always constrained by field data. The volume diverged by 25%, corresponding to a volume of 3.9 km^3. The total CI volume uncertainties are 5.5 km^3.